

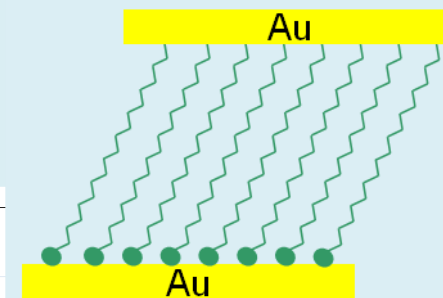
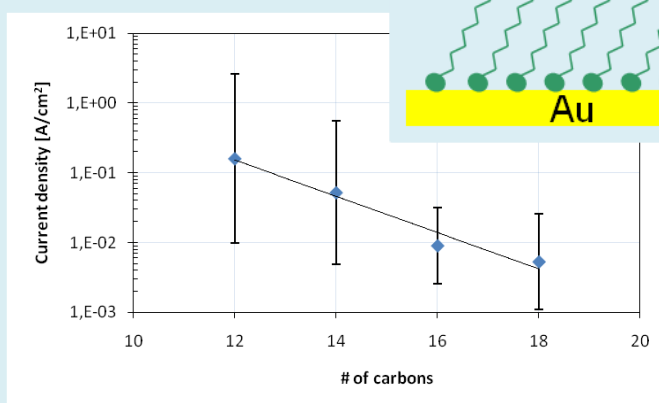
The Flip-chip concept:

A new way to electrically characterize molecular monolayers

Master thesis

Janine Wilbers

22/07/2011 Enschede



Committee members:

Supervisor: Prof. dr. ir. Wilfred G. van der Wiel

Daily supervisor: Sven Krabbenborg MSc

Member: Prof. dr. ir. Jurriaan Huskens

External Member: Dr. Edwin T. Carlen

Abbreviations

AFM	Atomic force microscope
CA	Contact angle
DI water	Deionized water
EGaIn	Eutectic gallium indium
HF	Hydrofluoric acid
HOMO	Highest occupied molecular orbital
IPA	Isopropyl alcohol, 2-propanol
LOFO	Lift-off, float-on
LUMO	Lowest unoccupied molecular orbital
NMR	Nuclear magnetic resonance
MLG	Multilayer graphene
OA	Optical adhesive
PALO	Polymer-assisted lift-off
PDMS	Poly (dimethylsiloxane)
PEDOT:PSS	Poly (3, 4-ethylenedioxythiophene) stabilized with Poly (4-styrenesulfonic acid)
PFDTs	1H, 1H, 2H, 2H-Perfluorodecyl-trichlorosilane
PMMA	Poly (dimethyl methacrylate)
rms roughness	Root-mean-squared roughness
PPF	Pyrolysed photoresist film
PRS	Positive resist stripper (PRS 2000)
RT	Room temperature
SAM	Self-assembled monolayer
SDMD	Surface-diffusion-mediated deposition
SEM	Scanning electron microscope
TEM	Transmission electron microscope
UV	Ultraviolet

Abstract

The biggest challenge in the fabrication of molecular monolayer junctions is the application of the top contacts without damaging the molecules. To allow statistical analysis of the molecular junctions they have to yield reliable and reproducible results. There are already several techniques for the fabrication of molecular monolayer junctions, but all of them have their own disadvantages like low yields or uncertainties in the junction system when an additional layer is introduced between the molecules and the top electrode. Until now no successful fabrication technique has been reported without a non-metallic layer between the molecules and the top contact.

In this Master thesis a new concept of molecular junction fabrication called flip-chip is presented. Hereby the top and bottom electrodes are fabricated at the same time and consist of the same metal. Self-assembled molecular monolayers are formed on smooth template-stripped Au electrodes. The top contacts are gently applied on top of the molecules by wedging transfer. The top electrodes are therefore coated with a hydrophobic polymer. When the device is dipped into water the electrodes embedded in the polymer are gently released from the wafer and float on the water. Removing of the water achieves a soft, non-destructive landing on the molecules. The electrode design allows the statistical electrical analysis of self-assembled monolayers in a short period of time for different junction area sizes. No additional layer was introduced between the self-assembled monolayers and the top electrodes, eliminating the ambiguities which occur for currently reported large-area molecular junctions.

Five different alkane-monothiols (from decanethiols (C_{10}) to octadecanethiols (C_{18})) have been characterized and compared to literature. The tunneling decay coefficient β was found to be 0.60 ± 0.11 per carbon atom (n_C^{-1}), which is slightly lower than the most recent β coefficients reported in literature (between 0.7 and $1 n_C^{-1}$). As wedging transfer is a water-based technique this lower value might be caused by water trapped in the junction. The current densities J measured for the different alkanethiols have a spread up to three orders of magnitude. This spread in J might indicate a limitation of the flip-chip concept. However, the origin is not yet known and has to be further investigated. In literature the reported J values have a mutual spread of up to eight orders of magnitude and our values lie approximately halfway in between.

Contents

1. Introduction and Motivation	9
2. Theory and State-of-the-art of molecular junctions	12
2.1. Molecules for molecular junctions	12
2.1.1. Self-assembled monolayers.....	12
2.1.2. Transport behavior of Alkanethiols.....	13
2.2. Fabrication of large-area molecular junctions	14
2.2.1. Lift-off, float-on (LOFO) and Polymer-assisted lift-off (PALO).....	15
2.2.2. Surface-diffusion-mediated deposition (SDMD)	16
2.2.3. EGaIn	17
2.2.4. Ga ₂ O ₃ /EGaIn stabilized in micro-channels in a transparent polymer (PDMS)	18
2.2.5. Au-SAMs-PEDOT:PSS/Au junctions.....	18
2.2.6. Molecular junctions with graphene flakes as top electrodes	19
2.3. Current densities <i>J</i> of molecular junctions shown in literature	20
3. Fabrication.....	23
3.1. Wedging transfer.....	23
3.2. Fabrication of the molecular junctions	24
3.3. Analysis of the metal electrodes	29
3.4. Characterization of the SAMs.....	33
4. Electrical measurements	35
4.1. Experimental results.....	36
5. Conclusions.....	46
6. Recommendations.....	47
6.1. Electrical measurements under vacuum.....	47
6.2. Embedding of the electrodes with PMMA instead of optical adhesive	47
Appendix 1.....	49
Appendix 2.....	51
References.....	52
Acknowledgements	55

1. Introduction and Motivation

Molecular electronics is an extending field of research since the publication by Aviram and Ratner in 1974 discussing how a single molecule can serve as a molecular rectifier¹. The basic idea of molecular electronics is the integration of organic molecules into electronic devices. Molecules are expected to exhibit various functionalities due to their different molecular structures². In the case of realizing a single molecule to function as an electronic device, like for example a rectifier, it is expected that Moore's Law can be extended by orders of magnitude compared to today's state of the art². Moore's Law predicts that the number of elements, which can be fabricated on one integrated circuit, doubles every two years^{3,4}. Although Moore's law still holds, it is hitting fundamental limitations. Industry requires low-cost production with excellent accuracy combined with increasing resolution. General photolithography is restricted to resolution (R) and depth-of-focus (DOF) given by equation 1 and 2:

$$R = k_1 * \frac{\lambda}{NA} \quad \text{Equation 1}$$

$$DOF = 0.5 * k_2 * \frac{\lambda}{NA^2} \quad \text{Equation 2}$$

where k_1 and k_2 are the imaging constants, λ is the exposure wavelength, and NA is the numerical aperture⁵. Increasing of the resolution of optical lithography with acceptable DOF has been tried with shorter wavelength exposure. Wavelengths below 193 nm (deep-UV/ DUV) lead to restrictions to imaging optics and resist systems. Next to the scaling limitations of photolithography also the costs for more sophisticated equipment are rising. To meet industrial requirements next generation lithographic technologies are needed like for example imprint lithography. Another promising strategy to pursue Moore's law is molecular electronics.

Figure 1 shows three fields in which molecular electronics can be differentiated from conventional

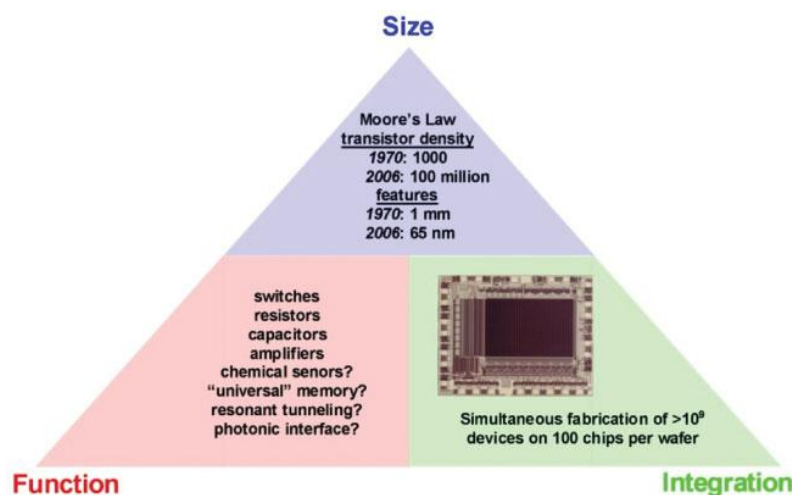


Figure 1. Three areas of molecular electronics illustrating advantages over conventional electronics².

electronics². With smaller size and higher levels of integration it is possible to make use of increased parallel operation within one integrated circuit, while molecular functions allow new applications and improved performance. To introduce organic molecules into electronic devices, reliable methods are required for investigating the electronic transport properties of those molecules. It is hard

to reliably fabricate single molecule devices and yet get statistically relevant data. Therefore, a step back is taken and first an ensemble of molecules is analyzed. Self-assembled monolayers (SAMs) form spontaneously from solution or the gas phase onto the surface of noble metals. Very common SAMs are alkane-(di) thiols on Au, Ag, and Pt. The layer thickness is typically 1-3 nm. SAMs are very

suitable for characterization studies because they are easy to prepare, a monolayer is formed on all kinds of substrate shapes, and they can serve as binding blocks between two metal contacts⁶. To measure the conductance of organic molecules, it is necessary to contact the molecules between two electrodes. A variety of fabrication methods for molecular junctions are reported, ranging from single-molecule junctions (break junctions⁷) and small junction areas contacted with scanning tunneling or conducting probe atomic force microscopy to large-area molecular junctions². The challenge of the formation of molecular junctions is the application of the top contact. Direct metal evaporation of the top electrode on top of a SAM leads to metal filaments through the monolayer causing shorts. The yield of one such approach was reported to be $\sim 1.2\%$ ⁸. Higher yields were achieved with eutectic gallium indium (EGaIn) as top electrode⁹, as well as introducing a conductive polymer layer between the SAM and the top contact¹⁰. The drawbacks of such methods are that additional resistances like Ga_2O_3 for the EGaIn technique as well as the conductive polymer have an influence on the conductance measurements. The conductive polymer has a non-negligible resistance so that it is not possible to measure alkanethiols shorter than tetradecanethiols (C_{14}).

In this Master project, the flip-chip concept (see Figure 2) developed in the NE and MnF groups is

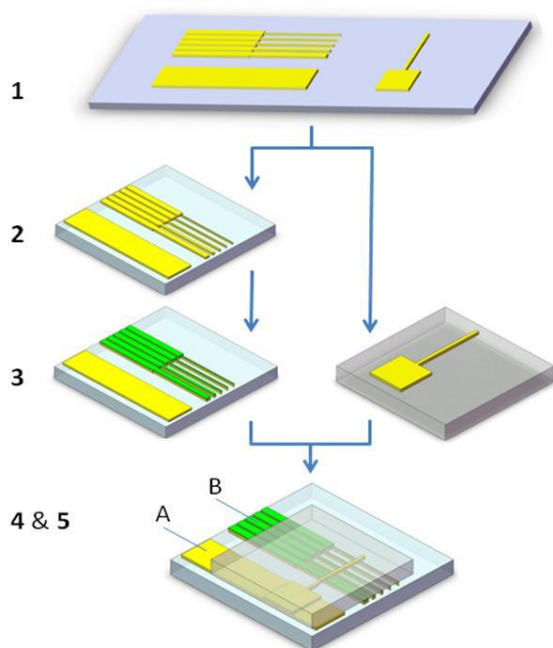


Figure 2. Fabrication steps of the general flip-chip concept; yellow: Au electrodes, green: SAM, dark blue: Si wafer, light blue: glass slide, grey: PDMS stamp. 1) evaporation of the Au electrodes on a Si wafer; 2) template-stripping of the top contacts by means of optical adhesive; 3) formation of SAM from solution on the bottom electrodes and template-stripping of the top contacts; 4+5) flipping of the PDMS stamp and positioning of the top electrodes on the molecular monolayer, I-V measurements are made by contacting the molecular junction at points A and B¹¹.

used to fabricate molecular junctions with alkanethiols¹¹. The fabrication scheme is based on metal lift-off and template-stripping. A poly (dimethylsiloxane) (PDMS) stamp was originally patterned with Au contacts and applied on top of the bottom contacts covered with the SAM. The working device yield was $\sim 10\%$. Compared to other methods the flip-chip concept has a number of possible advantages. It allows easy and fast fabrication of a large number of molecular junctions on one device. The electrode surfaces are characterized by a low roughness minimizing damage to the molecular monolayer. The bottom and top electrodes are fabricated at the same time and consist of the same metal. No additional layer between the molecules and the top electrode is needed. The electrodes are designed so that scaling in junction area is achieved which is useful for statistical analysis.

The aim of this project is to improve the flip-chip method to enhance the working device yield of the flip-chip concept and to reduce the large spread in current densities measured through alkanethiols to achieve reliable electrical characterization of the molecules.

The state of the art of molecular junction fabrications is summarized and the electrical properties of alkane-monothiolis measured with the different techniques are compared in Chapter 2. A softer landing technique for the application of

the top contact called wedging transfer is described in Section 3.1. The softer landing is expected to reduce damage to the monolayer and thereby allow higher yields and less spread in current densities. Electrical characterizations of five alkane-monothiols are described and compared with literature. In the end conclusions are drawn and recommendations are given in Chapter 6.

2. Theory and State-of-the-art of molecular junctions

2.1. Molecules for molecular junctions

The molecular junctions studied in this project, are formed with self-assembled monolayers of alkane-monothiois. Thiols have a strong affinity to noble metals like Au, Ag, and Pt, allowing a densely packed monolayer formation on the bottom electrodes. The contact to the top of the SAM is formed via physisorption of the CH₃-endgroup to the Au top contact.

2.1.1. Self-assembled monolayers

Self-assembly means that a disordered system spontaneously forms an assembly in a thermodynamic minimum with a definite, limited degree of order¹². One of the most famous phenomena of self-assembly are SAMs¹³. SAMs are molecular monolayers that self-assemble spontaneously on a surface when the substrate is immersed in an organic solution containing the thiols¹⁴. Hereby the active surfactants of the molecules adsorb on a metallic substrate and form ordered assemblies of molecules¹³.

The general structure of alkanethiol self-assembled monolayers consists of three main building blocks:

- the ligand or head group
- the alkane chain
- the terminal functional group

In Figure 3 a SAM of alkanethiolates formed on an Au (111) substrate is schematically shown. The ligand or head group of the alkanethiolates has a high affinity to the gold substrate.

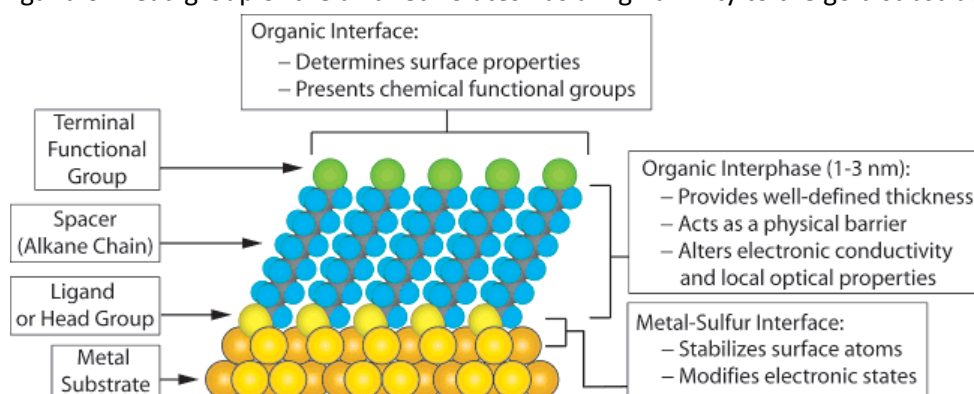


Figure 3. Schematic picture a of self-assembled monolayer with the three building blocks: head group, alkane chain and terminal functional group; the molecules (alkanethiolates) self-assemble on an Au (111) substrate and form a densely packed monolayer⁶.

The head group forms the chemisorption to the surface of the solid substrate, which is the most exothermic process¹⁴. This chemical bond in the case of alkanethiols on gold is a covalent, but slightly polar, Au-S bond¹⁴. The corresponding energies of the chemisorption process are about 40 – 45 kcal/mol for alkanethiols on gold. When more molecules are bound to the substrate they rearrange, forming the ordered monolayer¹⁴. This is because the molecules aim to occupy each free binding site on the substrate surface¹⁴. When the molecules are close enough together, short-range forces (Van der Waals forces) can be formed¹⁴. The alkyl chain forms interchain interactions via Van der Waals forces with energies ≤ 10 kcal/mol. The terminal functional group also has an influence on the packing density and the organization of the molecular monolayers⁶.

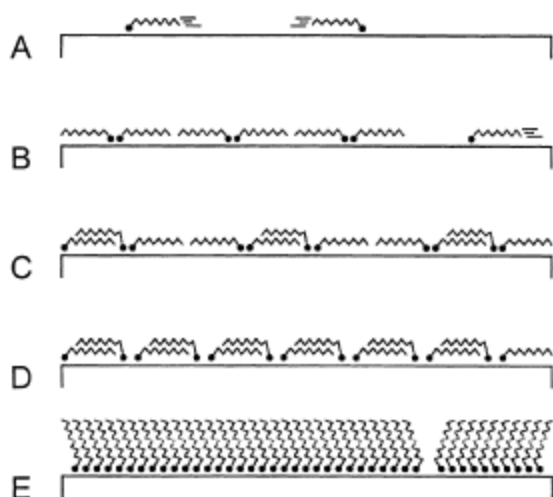


Figure 4. Different phases during monolayer formation of decanethiols on Au: A-D: lying-down phase and E: standing-up phase¹⁵.

Depending on the thiol concentration, the molecules can have a standing-up phase for a high concentration or a lying-down phase for a low concentration. During the growth of the molecular layer the molecules are first in a lying-down phase before they end up in a final standing-up phase¹⁵.

2.1.1.1. Alkanethiols/ Alkanedithiols

Alkane(di)thiols have a strong affinity to gold. In this thesis alkane-**monothiols** will be used to fabricate molecular junctions. They form more reliable organized and densely packed monolayers than alkanedithiols. In the case of alkanedithiols the possibility for defects is larger, as they have two chemisorbing head groups. If the molecular chains are long, the two head groups can both bond to the bottom electrode forming a laying-down phase or a loop if the chain is long enough instead of standing-up, which is needed for a dense packing monolayer.

2.1.2. Transport behavior of Alkanethiols

The charge transport mechanism through SAMs of short alkanethiols (< 3 nm) is tunneling. An evidence for tunneling transport is that the current densities show an exponential dependence on molecular chain length. This means that with increasing chain length the tunneling current decreases. The tunneling current densities are independent of temperature¹⁶. This behavior is observed for alkane-monothiols as well as for alkane-dithiols. Alkane(di)thiols have an energy gap of 8-10 eV between the highest occupied molecular orbital (HOMO) and the lowest unoccupied molecular orbital (LUMO), which makes them behave as insulating materials¹².

Physisorbed and chemisorbed contacts of the same chain lengths show different values in conduction up to several orders of magnitude, which means that the conduction through monothiols and dithiols will differ significantly¹². We could give an explanation for this in terms of the Landauer equation:

$$G = \frac{2e^2}{h} \times T_t \times T_{mol} \times T_b, \quad \text{Equation 3}^{12}$$

where G is the conductance, e the elementary charge, h the Planck's constant, and T_t , T_b and T_{mol} are the respective probabilities of transmission through the top contact, the bottom contact and the molecule. The transmission coefficients are different for CH_3 and SH termination, which occur

respectively for physisorbed and chemisorbed contacts. When the transmission of one contact is varied, the conduction of the whole system is changed as well¹².

Hopping transport is characterized by an I - V behavior that depends on temperature. This dependence is given by:

$$\ln\left(\frac{V}{J}\right) \sim \frac{1}{T} \quad , \quad \text{Equation 4}^{17}$$

where J is the current density, V is the voltage and T is the temperature. This transport mechanism is mainly valid for molecules longer than 3 nm and is characterized by a linear scaling with weak length dependence of the conductance^{18,19}.

The current density through a molecular junction with short molecules depends exponentially on the chain length of the molecules. By plotting the current densities at a given voltage as a function of molecular length the tunneling decay coefficient can be obtained from the slope of the exponential fit. This is an approximation of the Simmons equation given by:

$$J = J_0 e^{-\beta d} \quad , \quad \text{Equation 5}^9$$

where J is the current density [A/m^2], β is the tunneling decay constant [\AA^{-1} or n_c^{-1} (number of carbons)] and d is the thickness of the SAM [\AA or n_c]. J_0 is a constant which is dependent on the device and it takes the contact resistance into account¹⁶. It is the current density across an imaginary monolayer without an alkyl chain which means $d=0$. It can be calculated by the interface between the electrode contacts and the monolayer⁹.

The tunneling decay coefficient β gives information about the degree of decrease in the wave function of the electron that tunnels through the molecular backbone²⁰. Most decay coefficient values reported in literature for even-numbered alkanethiols are between 0.71 and 1.1 \AA^{-1} ⁹.

2.2. Fabrication of large-area molecular junctions

In literature many ways to electrically characterize SAMs are reported. Methods to analyze small numbers of molecules or even single molecules are using scanning probe methods, break junctions, metallic cross-bars or nanopores¹⁰. The conductance per molecule differs by orders of magnitude²¹. It is difficult to fabricate reliable single molecule junctions and yet get statistically relevant data. Therefore, a step back is taken by forming large-area molecular junctions which are more suitable for the characterization of molecules. The resulting conductance is averaged over many molecules and thereby includes variations in tunneling current²¹.

It is very challenging to fabricate devices in which the SAMs are placed between two metal electrodes. This is due to the fact that by conventional metal evaporation of the top layer on the SAMs (with a thickness of ~ 1 -2 nm depending on the molecule²²), the metal atoms penetrate the molecular layer and make contact with the bottom electrode. This causes shorts and reduces the working device yield dramatically to 1.2%⁸. For the application of SAMs in electronic devices the molecular junctions have to be stable, reliable and show a higher working device yield²³.

Below different methods for large-area molecular junction fabrication are presented.

2.2.1. Lift-off, float-on (LOFO) and Polymer-assisted lift-off (PALO)

In the lift-off, float-on process (LOFO) a thin metal film is gently transferred onto a solid substrate. The metal film is first evaporated onto a support to which it forms weak adhesion and then lifted-off in a liquid medium. The metal layer is drifting on the liquid. During the floating-on step the metal film can be attached to the bottom substrate with the molecular layer²⁴.

The drawback of this method is that the detached solid film often wrinkles during making contact with the substrate²⁴.

Polymer-assisted lift-off (PALO) is an improvement of the LOFO process. With PALO the problem of wrinkling is solved by using a polymer backing layer usually consisting of poly(dimethyl methacrylate) (PMMA) which is spin-coated on the metal electrodes²⁵.

In earlier PALO methods punches had to be made through the polymer backing layer to allow contact of the probes with the metal for electrical measurements. With the recently published modified PALO method this disadvantage is overcome by using a photoresist instead of the PMMA which can be structured with lithography²⁵.

In the first step, metal structures are evaporated onto a sacrificial substrate with a shadow mask. On top of these metal structures a layer of hydrophobic photoresist is spin-coated, which is subsequently patterned with holes above the metal pads by photolithography. To allow lift-off the whole device is first dipped into 2% hydrogen fluoride to etch the SiO₂ of the Mica substrate. Lift-off is done in deionized (DI) water and the drifting photoresist/metal pads devices are floated onto a previously prepared substrate. The whole process is schematically shown in Figure 5. The electrical measurements are done with probes that are placed inside the holes of the backing layer making contact to the metal film. The contact area size is consequently limited and permanent electrical contacts via wire bonding are not possible²⁵.

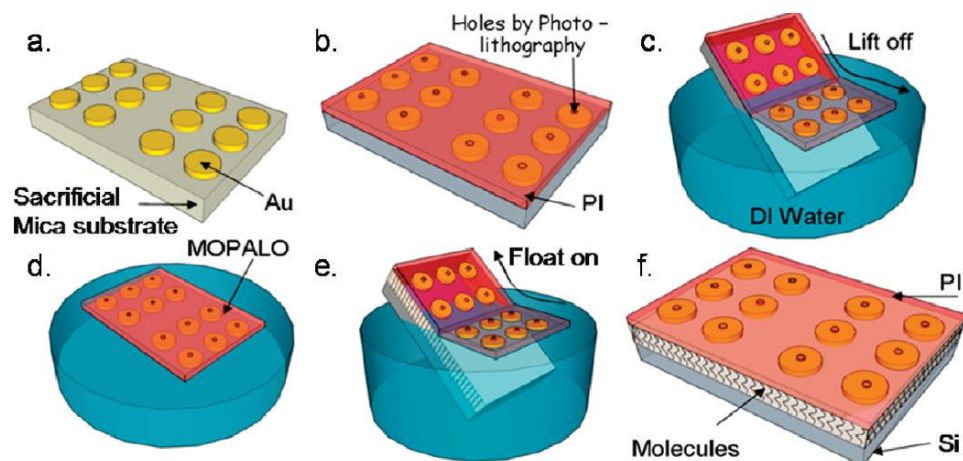


Figure 5. Schematic of the modified polymer-assisted lift-off process; (a) evaporation of the metal electrodes, (b) spin-coating of the photoresist (polyimide PI) and fabrication of the holes via photolithography, (c) lift-off of the PI and the electrodes, (d) PI/electrodes are floating on the water, (e) PI/electrodes are floated on the substrate, and (f) final molecular junction²⁵.

Another form of the modified PALO method is permanent modified PALO which allows wire bonding and smaller contact areas. Permanent leads are formed to contact the metal outside the holes (Figure 6). The electrical contacts are made with wire bonding.

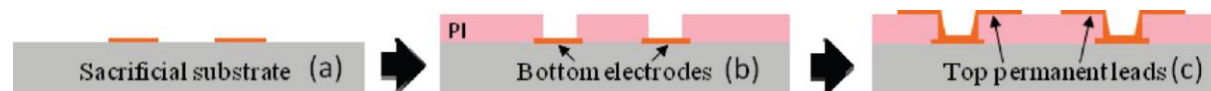


Figure 6. Fabrication of top permanent leads for permanent modified PALO²⁵.

The additional evaporated metal in the permanent modified PALO method makes the photoresist/metal layer stiffer. Therefore, water has to be replaced by a volatile solvent. As the photoresist/metal layer has a lower surface tension it cannot float on water. A two-phase system of water-methanol and ethyl acetate is therefore utilized. The layer floats at the liquid/liquid interface and is taken through the ethyl acetate to the bottom contact. After this, the whole device is dried with N_2 ²⁵. For the modified PALO it was reported that water was trapped after the floating step. It cannot be excluded that also here trapped water may influence electrical measurements.

2.2.2. Surface-diffusion-mediated deposition (SDMD)

Surface-diffusion-mediated deposition (SDMD) is another method for soft deposition of the top metal contact. Hereby a SiO_2 overhang is constructed to avoid direct evaporation of metal atoms and source radiation. Via surface diffusion of Au adatoms on the SiO_2 surface the metal atoms form the Au layer above the monolayer. At the edges of the metal film diffusing adatoms are incorporated and as a result the edge migrates into the direction of the molecular film. The working device yield was higher than 90%²⁶. Figure 7 shows the fabrication process of SDMD.

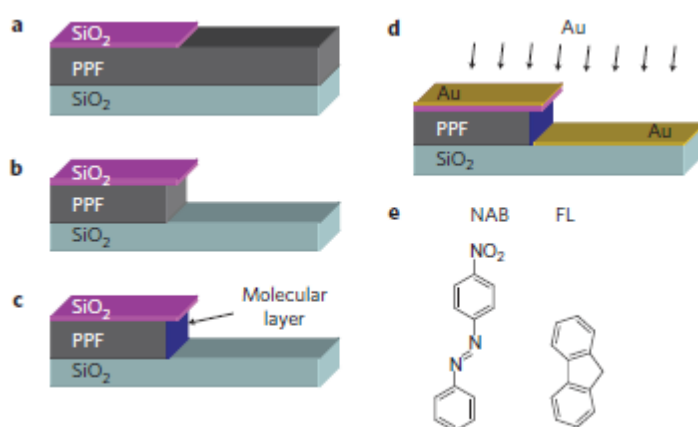


Figure 7. Schematic image of the surface-diffusion-mediated deposition (SDMD); a) formation of a SiO_2 etch mask on a pyrolysed photoresist film (PPF) by photolithography, b) by utilizing O_2 reactive ion etch a sidewall is formed, c) formation of a molecular layer on the PPF, d) deposition of Au and formation of the metal top contact via Au surface diffusion²⁶.

The contact area of the molecular junction is ~ 1 μm broad and ~ 150 nm high. The height is the diffusion length onto the molecules and was determined by scanning electron microscopy. This is a disadvantage of the system as the determination of the diffusion length has to be determined for each test chip with 6 to 9 molecular junctions on one chip. The current through the molecules is measured by forming contact leads on the pyrolysed photoresist film (PPF) as well as the SiO_2 before Au evaporation.

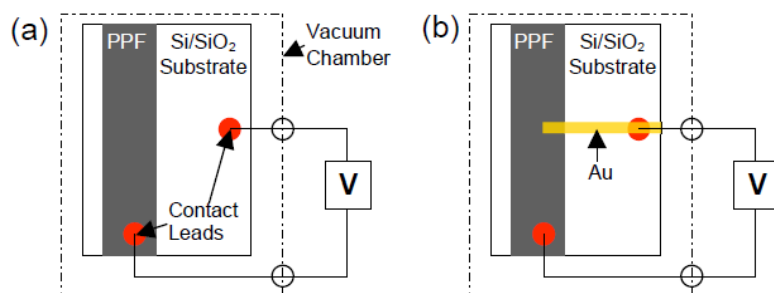


Figure 8. Schematic of the characterization set-up for molecular junctions formed with SDMD; (a) Formation of contact leads on PPF and SiO₂, (b) Au deposition with a shadow mask²⁶.

2.2.3. EGaIn

Eutectic gallium indium (EGaIn; 75.5 wt% Ga and 24.5 wt% In) is a material to characterize charge transport through monolayers. At room temperature it forms metastable, nonspherical structures with a diameter $\geq 1\mu\text{m}$ while it stays liquid^{9,27}. With a melting point of 15.5°C EGaIn is liquid at room temperature, but it does not reflow into a shape with the lowest free energy like for example water does. Just after a critical surface stress of 0.5 Nm^{-1} it begins to flow²⁷. When EGaIn gets into contact with oxygen it forms a $\sim 1\text{ nm}$ thick Ga₂O₃ layer which permits EGaIn to preserve the stable, conical shape while it stays deformable during contacting with hard surfaces⁹. These properties as well as the high electrical conductivity ($3.4 \times 10^4\text{ S}\cdot\text{cm}^{-1}$) of EGaIn and its tendency to form interfaces with low contact-resistances make EGaIn suitable for top contacts on top of molecules²⁷. As bottom contacts template-stripped metal electrodes are used on which the SAM is formed. Schematics of an EGaIn set-up and the molecular junction area are shown in Figure 9.

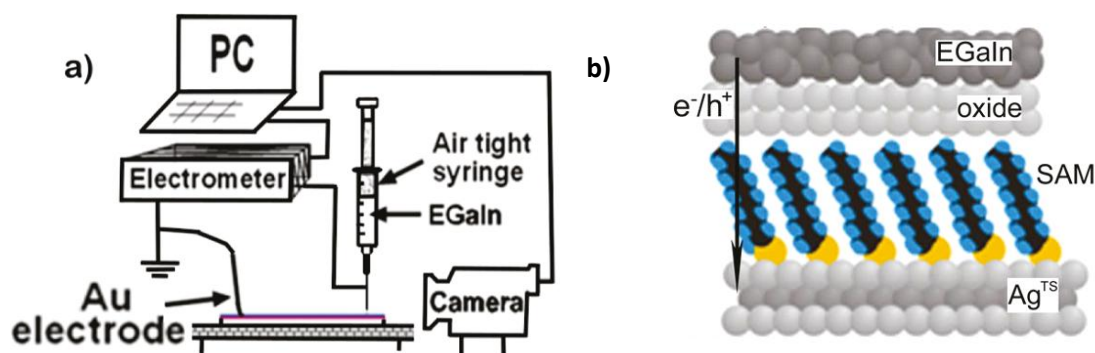


Figure 9. a) EGaIn measurement set-up; b) cross-section of a molecular junction with template-stripped Ag as bottom electrode and Ga₂O₃/EGaIn as top contact⁹.

The working device yield of these junctions is reported to be 80%. Whitesides et al.⁹ attributed the high yield to the oxide layer because it prevents metal filaments like a conductive polymer film in other molecular junction fabrication techniques¹⁰. On the other hand this oxide layer is an additional tunnel barrier that influences the current density values. The electrical resistivity of Ga₂O₃ is about three orders of magnitude lower than that of nonanethiols (C₉). Over an area of about $1\mu\text{m}$ the roughness of the oxide film makes it difficult to approximate the real contact area. Furthermore, molecules can be detached from the Ag substrate and stick to the Ga₂O₃/EGaIn. The consequence of this contamination on the current densities is not known. As these two effects are the same for different kinds of alkanethiols it is assumed that the results are reliable because they are reproducible and the β coefficient of 1.15 n_c^{-1} is comparable to literature⁹.

2.2.4. Ga₂O₃/EGaIn stabilized in micro-channels in a transparent polymer (PDMS)

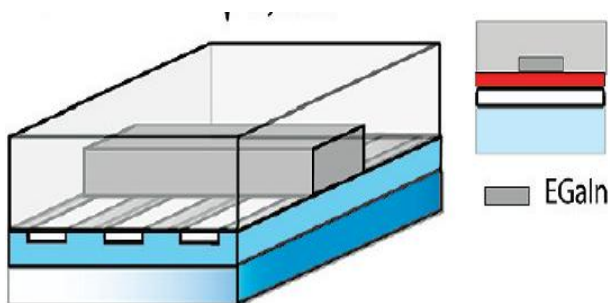


Figure 10. Schematic of a molecular junction fabricated with template-stripped bottom electrodes and Ga₂O₃/EGaIn inside a microchannel in PDMS; explanation of the colors: light grey = PDMS, red = SAM, white = Ag electrode, light blue = optical adhesive, blue = glass¹⁶.

J-V measurements were carried out with alkane-mono-thiols of C₁₂, C₁₄, C₁₆ and C₁₈ as well as alkanethiolates with ferrocene ending groups. The latter ones can be used as molecular diodes. The current densities of molecular junctions with EGaIn as top electrode have uncertainties compared to junctions with metal top contacts. EGaIn forms a Ga₂O₃ layer when it gets into contact with oxygen. The authors assume that the resistance and thickness nearly have no influence to the *J-V* measurements. They conclude this because the Ga₂O₃ layer is thinner than 2 nm with a resistance 3 orders of magnitude less than measured for alkanethiols.

2.2.5. Au-SAMs-PEDOT:PSS/Au junctions

A method to fabricate very stable molecular junctions with a working device yield of > 95% was shown by Bert de Boer et al¹⁰. They have overcome the difficulties that are associated with direct

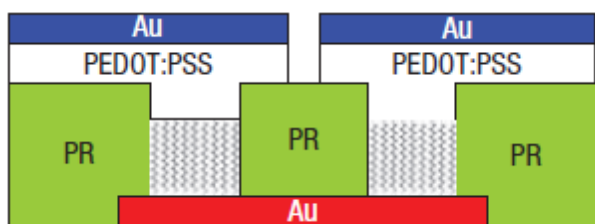


Figure 11. Schematic image of a cross-section of a molecular junction Au/SAM/PEDOT:PSS-Au²³.

The 40 nm thick bottom Au electrodes are formed on a Si wafer with a 2 nm thin chromium adhesion layer. In the next step a photoresist is spin-coated and holes are structured with optical lithography. The contact areas on which the SAM is formed are between 0.8 and 2,000 μm². The top electrode is fabricated by first spin-coating a layer of PEDOT:PSS and then evaporating Au through a shadow mask. Reactive ion etching is used to remove the exposed PEDOT:PSS.

Next to the high working device yield these junctions provide also stable *I-V* measurements even after storage under ambient conditions over 2.5 years. After 288 days of storage the resistance change is less than a factor of two²⁸.

Also large-area measurements with EGaIn were reported by G. M. Whitesides et al¹⁶. These tunneling junctions are made of template-stripped Ag bottom electrodes covered with self-assembled monolayers. For the top electrodes microchannels are fabricated in PDMS. These channels are filled with Ga₂O₃/EGaIn forming the top contact. A schematic picture is shown in Figure 10. With this method it is not necessary to evaporate the top contacts and therefore metal penetration through the monolayer is avoided. It is possible to make electrical

measurements at different temperatures and with different molecular lengths. The working device yield was reported to be 70-90 %.

evaporation of the metal electrodes by introducing a conducting polymer on top of the SAM before evaporation of the top contact. As conductive polymer poly(3,4-ethylene-dioxythiophene) stabilized with poly(4-styrenesulphonicacid) (PEDOT:PSS) with a conductivity of 30 S*cm⁻¹ is used¹⁰. A schematic picture of these molecular junctions is shown in Figure 11.

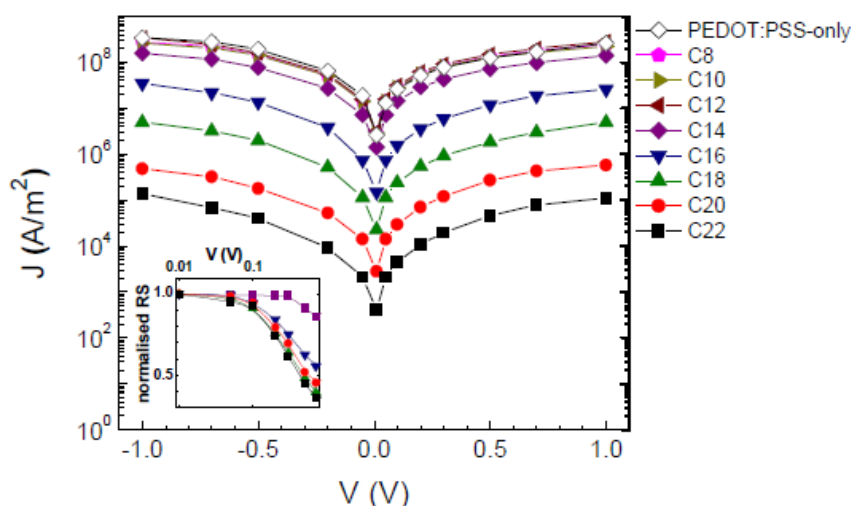


Figure 12. *J-V* curves of Au/SAM/PEDOT:PSS-Au molecular junctions compared to a Au/PEDOT:PSS-Au junction only; for alkane-mono-thiols with chain lengths longer than C₁₄ the current densities can be distinguished from a PEDOT:PSS-only junction²⁹.

the polymer film and the PEDOT:PSS is more repelled from the SAM¹². Therefore, the current densities of alkane-mono-thiols have a slightly higher standard deviation than alkane-dithiols²⁹ but still it is currently one of the most reliable, stable systems concerning the stability of measured current density compared to other large-area molecular junction fabrication techniques^{9,16,30}.

2.2.6. Molecular junctions with graphene flakes as top electrodes

Recently, a fabrication scheme of molecular junctions based on Au-SAM-graphene/Au was reported by Gunuk Wang et al³⁰ (see Figure 13). The molecular monolayer is formed on Au bottom electrodes that were evaporated on a Si/SiO₂ wafer. The diameter of the contacts is 4 μm. A multilayer graphene (MLG) flake is positioned above the junction area. Graphene is a 1-atom thin 2D leaf of carbon atoms that are covalently bonded. Its chemical, electrical and mechanical properties are excellent. For the Au-SAM-graphene/Au junctions a MLG is used. In the last step Au electrodes are formed with vapor-deposition through a shadow mask. Metal filaments and shorts are reduced by the graphene flake. The working device yield for alkane-monothiols and alkane-dithiols was reported to be around 90%.

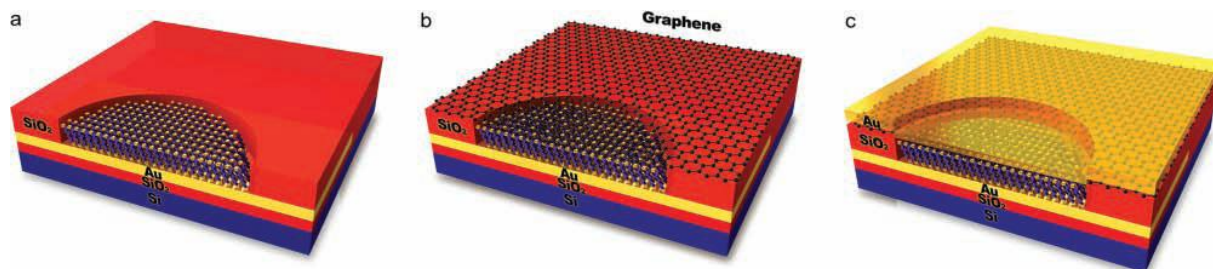


Figure 13. Fabrication scheme of molecular junctions with a multilayer graphene flake as top electrode [25]. a) – c) fabrication steps of the molecular junctions³⁰.

The authors report that the contact conductance of SAM-graphene is better than SAM-PEDOT:PSS. Nevertheless, asymmetrical electrodes are fabricated by introducing an additional layer of up to 10 nm between the molecules and the Au top contact.

These molecular junctions have two disadvantages, though. First of all, the current densities *J* of short alkane-mono-thiols (C₈, C₁₀, C₁₂) cannot be distinguished from junctions only with PEDOT:PSS as shown in Figure 12.

Secondly, the hydrophobic CH₃ ending groups of alkane-mono-thiols make it difficult to form molecular junctions with a PEDOT:PSS-Au top contact as this polymer is hydrophilic^{10,12}. Spin-coating of PEDOT:PSS on the CH₃ end of alkane-mono-thiols can lead to pinholes in

2.3. Current densities J of molecular junctions shown in literature

In this section the current densities J [A/cm²], working device yields [%] and the spread in J [orders of magnitude] for one chain length of alkane-monothiols from each reference are summarized and discussed.

In Table 1 the working device yields [%] for different kinds of fabrication methods are shown. The yields are quite high with between 70 and 95%. However, none of these molecular junctions have bottom and top electrodes made with the same material. All these fabrication techniques either introduce an additional layer like the conductive polymer PEDOT:PSS or a multilayer graphene film before evaporation of the top layer. This is done in order to avoid shorts originating from filament growth of the evaporated top contact through the monolayer.

Table 1. Working device yield [%] and decay coefficient values for different types of molecular junctions.

Method	Junction area [μm^2]	Working device yield [%]	Decay coefficient β_N (per carbon)
Au-SAM-PEDOT:PSS/Au ²⁹	0.8 – ~2,000	95	0.9
Ag ^{TS} -SAM-Ga ₂ O ₃ /EGaIn ⁹	~ 500	80	1.024 ± 0.092 (at -0.5 V)
Ag ^{TS} -SAM-Ga ₂ O ₃ /EGaIn in microchannel ¹⁶	300	70 - 90	1.0 ± 0.2 (at 0.5 V)
Au-SAM-graphene/Au ³⁰	0.126	90	1.06 ± 0.14 (at 1 V)

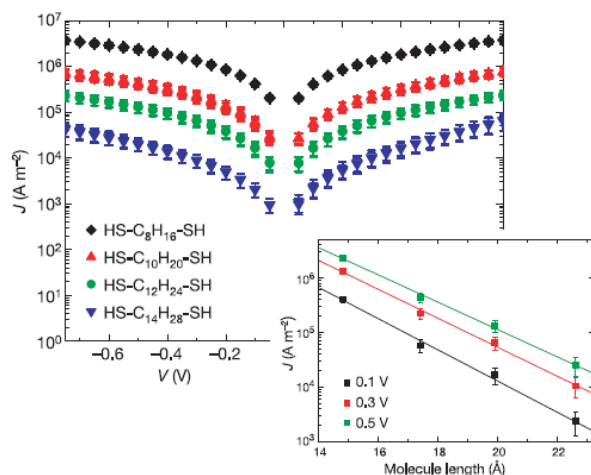
As described in paragraph 2.1.2, the current density through a molecular junction depends exponentially on the chain length d of the molecules: $J = J_0 e^{-\beta d}$. The decay coefficient values are all around 1/C atom. A comparison of decay constants was already discussed earlier in literature¹². In that report also single molecule junctions like molecular break junctions as well as measurements performed with scanning tunneling spectroscopy (STM) were included in the list. The decay constants ranged between 0.51 and 1.16 per C atom with 0.92 ± 0.19 per C atom on average. No reason was found to explain the large spread in decay coefficients which most probably indicates that the measured current densities depend on the different junction devices.

Next to the decay constants it is also interesting to look at the current densities measured with different molecular junction devices. The averaged current densities J for different alkane-monothiols are reviewed in Table 2. From this table it can clearly be seen that the contacts to the molecules are crucial for the electrical characterization of SAMs. For the same molecular length but different electrode materials the current densities differ up to eight orders of magnitude like for C₁₆ and C₁₈.

Table 2. Current density J [A/cm^2] at 0.5 V reported in literature for different chain lengths of alkane-monothiol.

Method	Junction area [μm^2]	C_8	C_{10}	C_{12}	C_{14}	C_{16}	C_{18}	C_{20}	C_{22}
Au-SAM-PEDOT:PSS/Au ²⁹	0.8 – ~2,000				$9 \cdot 10^3$	$1 \cdot 10^3$	$2 \cdot 10^2$	$2 \cdot 10^1$	$4 \cdot 10^0$
Ag^{TS} -SAM- $\text{Ga}_2\text{O}_3/\text{EGaIn}^9$	~ 500		$2 \cdot 10^{-2}$	$4 \cdot 10^{-3}$	$2 \cdot 10^{-4}$	$4 \cdot 10^{-5}$	$5 \cdot 10^{-6}$		
Ag^{TS} -SAM- $\text{Ga}_2\text{O}_3/\text{EGaIn}$ in microchannel ¹⁶	300			$3 \cdot 10^{-4}$	$1 \cdot 10^{-4}$	$1 \cdot 10^{-5}$	$2 \cdot 10^{-6}$		
Au-SAM-graphene/Au ³⁰	0.126	$6 \cdot 10^4$		$1 \cdot 10^3$		$9 \cdot 10^0$			

In Table 3 the current density standard deviations for various lengths of alkanethiols and the different fabrication techniques are listed. The values were taken from the error bars obtained with the log-standard deviations for all three methods. For the J - V plots of Au-SAM-PEDOT:PSS/Au with alkane-monothiols the standard deviation has not been shown in the articles or supporting information. However, it was shown for the same molecular junction device with alkane-dithiols.

**Figure 14.** J - V curves and current densities at 0.1 V, 0.3 V and 0.5 V as a function of molecular chain length of Au-SAM-PEDOT:PSS/Au junctions¹⁰.

Hereby the standard deviation was very low, which can be seen in Figure 14. In reference [10]¹⁰ it was reported that Au-SAM-PEDOT:PSS/Au devices with alkane-monothiols reveal comparable current density versus voltage plots, but with a higher standard deviation.

The spreading in current density is quite high especially for molecular junctions based on EGaIn top electrodes. This might be caused by the roughness of the oxide layer which makes it difficult to determine the exact junction area. Furthermore, it is possible that the EGaIn is contaminated with molecules detached from the bottom contact, which also influences the measured values.

Table 3. Spread in current densities J for different chain lengths in orders of magnitude.

Method	Junction area [μm^2]	C_8	C_{10}	C_{12}	C_{14}	C_{16}	C_{18}
Ag^{TS} -SAM- $\text{Ga}_2\text{O}_3/\text{EGaIn}^9$	~ 500		0.6	1.7	2.1	1	1.3
Ag^{TS} -SAM- $\text{Ga}_2\text{O}_3/\text{EGaIn}$ in microchannel ¹⁶	300			0.5	0.8	1.1	0.9
Au-SAM-graphene/Au ³⁰	0.126	0.8		0.9		0.6	

In the Results and Discussion chapter, the measured J - V characteristics of the flip-chip devices for different chain lengths are compared and analyzed with the above mentioned junction devices.

3. Fabrication

The flip-chip concept was developed in the NanoElectronics Group and first realized by MSc student Sven Krabbenborg¹¹ in a joint project between the NanoElectronics and Molecular Nanofabrication groups, see Figure 2 in Chapter 1. The fabrication of the metal electrodes has three main steps, which are photolithography, metal evaporation and metal lift-off. The top and bottom electrodes for molecular junctions are template-stripped from a Si/SiO₂ wafer. The supports for the bottom contacts are glass slides while the ones for top contacts are PDMS stamps. PDMS stamps were utilized as they allow softer, non-destructive landing when positioned on top of the monolayer. The supports are applied with an UV-curable optical adhesive (OA). Template-stripped gold lines for bottom and top contacts have the advantage of ultra-flat surfaces³¹. The working device yield was ~10%. Hereby, the junction areas on one flip-chip device scale between 100 μm² to 40,000 μm².

The template-stripped electrodes were protruding from the optical adhesive which could maybe be one reason for the low yield. To overcome this it was recommended to use PMMA instead of the optical adhesive for template-stripping. Spin-coating of PMMA before applying the glass support by means of OA might cause less protrusion due to a better contact of the PMMA to the Au electrodes which would then overcome the problem of possible shrinkage of the OA. Another possibility is to try chemical Au etching. The etching rate is 3 nm/min. This should allow etching away the ~10 nm of protruding electrodes. Furthermore, the manual placement of the top electrodes might cause damage to the monolayer. To see if this is a reason for the low yield a softer landing technique should be tried. Different approaches of soft landing were therefore developed. One method to make gently contact with the SAM can be wedging transfer. The principle of wedging transfer is described in the next section.

3.1. Wedging transfer

Wedging transfer is a water-based method to transfer nanostructures onto diverse surfaces. The principle is similar to the PALO technique but it has not yet been used for the fabrication of molecular junctions. In the PALO technique a polyimide photoresist is utilized as a backing layer. The lift-off of the photoresist including the metal contacts is done in a 2% HF solution²⁵. Wedging transfer utilizes the hydrophobic effect meaning that water penetrates at the interface between hydrophobic and hydrophilic surfaces³². The detachment of the polymer including the metal electrodes is done in DI water. This is a non-toxic technique as no harmful acids are needed.

In the wedging transfer process, a hydrophobic structure is patterned on a hydrophilic surface such as SiO₂, mica, glass or quartz. The structured surface is covered with a hydrophobic polymer (cellulose acetate butyrate). By dipping the device into water under an angle of 30° or 150° the polymer including the pattern is wedged off from the hydrophilic substrate and floats on the water due to surface tension forces. If the angle is too high or too flat the polymer does not come off from the wafer. Subsequently, the structured polymer can be placed on a new substrate by releasing the water. The polymer film is positioned with probe needles. In the last step the polymer is dissolved in ethyl acetate leaving a nanostructure on the substrate. The whole process is schematically shown in Figure 15.

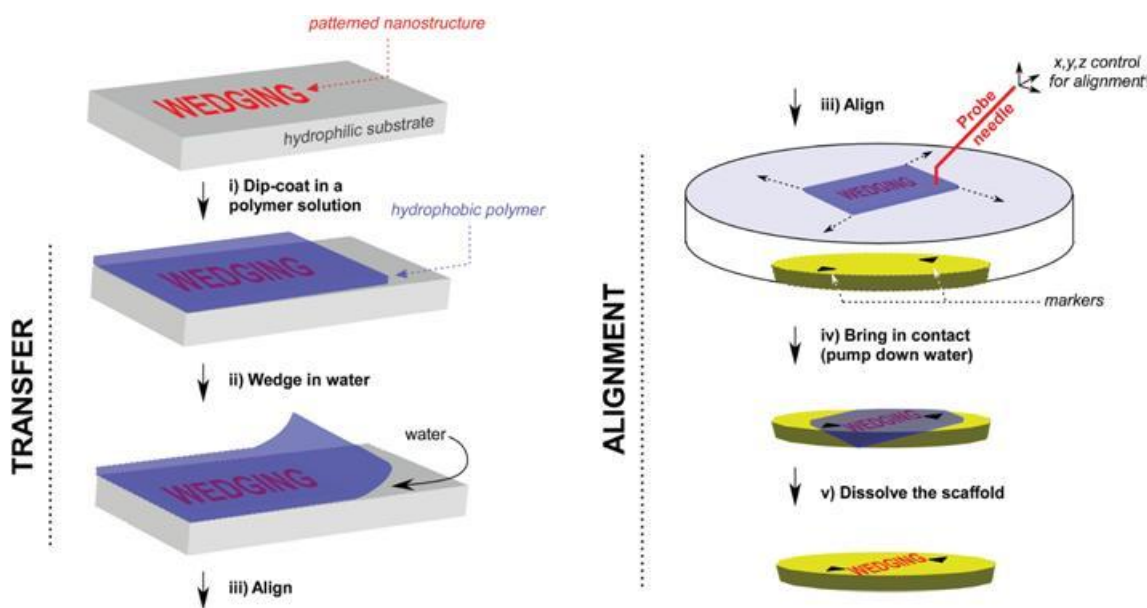


Figure 15. Schematic illustration of the process steps during wedging transfer. First a hydrophobic pattern is structured on a hydrophilic substrate and then covered with a hydrophobic polymer. The polymer with the pattern can be wedged off by dipping the device into water. By lowering the water level the nanostructure can be placed on the desired substrate and the polymer is dissolved with an adequate solvent³².

3.2.Fabrication of the molecular junctions

Lithography

In the first step, a single-side polished <100> silicon wafer is patterned by photolithography. The negative photoresist TI 35 ES (MicroChemicals) is spin-coated on the Si wafer. Subsequently the wafer is exposed with an inverse mask. An inverse mask means that the exposed areas remain after developing. Hereby a shorter exposure creates a larger undercut while a longer exposure forms steeper walls³³. The inverse mask design for top and bottom electrodes is shown in Figure 16.

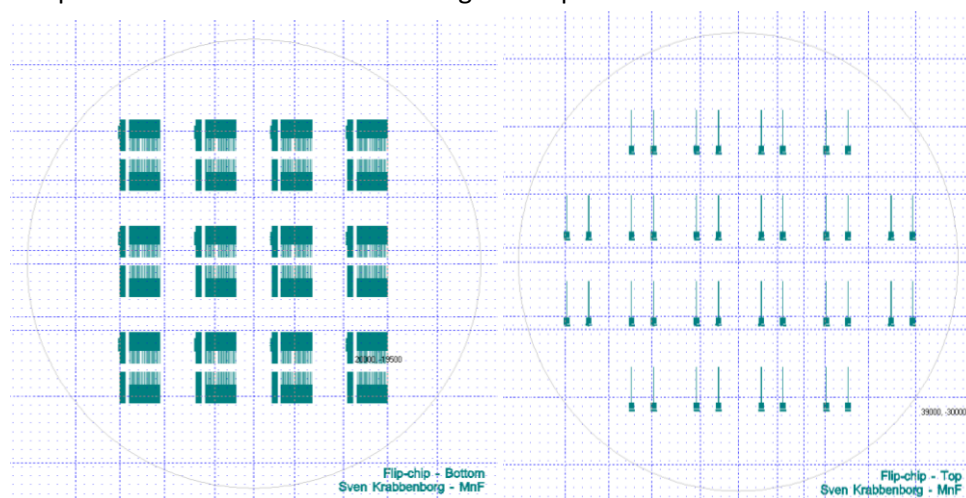


Figure 16. Photomasks for the bottom electrodes (left) and top electrodes (right) designed in Clewin.

In order to let the nitrogen (developed during exposure) diffuse out of the resist, the wafer is kept at room temperature for at least 30 min followed by a “reversal bake”. The reversal bake causes cross-linking of the irradiated area, while the unexposed area stays photo-active. In the next step a flood full wafer exposure is performed for 60 sec. Hereby, the parts of the resist layer that were not

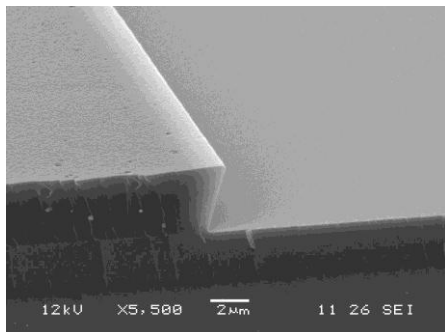


Figure 17. SEM image of the TI 35ES photoresist on a silicon wafer (Picture by Serkan Büyükköse MSc); with an exposure time of 20 sec an undercut of the photoresist is achieved.

exposed during the first exposure step, become soluble in the developer. The last lithography step is the developing in OPD4262 for 60 sec to remove the unirradiated area and subsequently quick dump rinsing with Milli-Q water. In the case of a negative resist the areas that are unirradiated will be removed during the developing step. The resist was imaged with scanning electron microscopy (SEM), which showed the formation of the desired undercut (see Figure 17). For the fabrication of the metal electrodes an undercut is favored to achieve metal electrodes with low edge roughness. For steep photoresist walls the metal is also deposited on the sidewalls causing rough electrode edges after the lift-off process. The metal evaporation and the lift-off process are explained below. A detailed description of the fabrication steps for electrodes fabrication is given in Appendix 1.

UV-ozone cleaning

To remove very thin resist films that remain on the wafer on the unirradiated areas after developing, 30 min UV-ozone cleaning is performed before the metal is evaporated. This step is very important to make template-stripping of the metal electrodes possible. Without UV-ozone cleaning the Au contacts remain on the wafer after template-stripping because the lithography changes the native oxide layer. UV-ozone cleaning gives a reliable initial situation with a thick enough native oxide layer before metal evaporation.

Electron-beam metal evaporation

The metal is deposited by e-beam evaporation (Film evaporator Balzers BAK 600). The thickness of the electrodes is 100 nm. Depending on the current [mA] the deposition rate is between 2 and 4 Å/s.

Metal lift-off

Metal lift-off was first done in acetone. Afterwards the wafers were rinsed with acetone and isopropyl alcohol (IPA) and spin dried. The lift-off time was varied between 60 min and 48 hours in order to get complete lift-off and clean electrode edges without remaining resist. It turned out that after lift-off for two days and also overnight the edges were not clean (see Figure 18). Further rinsing with acetone and IPA did not solve this problem. To analyze if the long metal lift-off time causes the contaminations on the edges of the electrodes the time was



Figure 18. Optical microscopy image of an Au electrode after metal lift-off in acetone overnight; at the edges of the electrode contaminations of remaining resist can be seen.

varied between 60 min and 48 hours in order to get complete lift-off and clean electrode edges without remaining resist. It turned out that after lift-off for two days and also overnight the edges were not clean (see Figure 18). Further rinsing with acetone and IPA did not solve this problem. To analyze if the long metal lift-off time causes the contaminations on the edges of the electrodes the time was

reduced. By scratching the metal layer between the electrodes, the metal lift-off can be speeded up. After 60 min the wafer is rinsed with acetone and IPA. The resulting electrodes also contained contaminations. Also higher temperatures during the lift-off process (40°C) did not eliminate the remaining resist.

The positive resist stripper (PRS 2000) is also suitable for lift-off of the TI 35 ES resist. The standard lift-off temperature for PRS 2000 is between 50-60 °C for 30 min. Due to the low adhesion of the Au to the Si performing lift-off under this condition is not possible, as most electrodes are removed from the wafer. Therefore, it was tried at room temperature (RT) which was also possible. A lift-off time of 60 min was found to be optimal. The Au layer was scratched between the electrodes to enhance the

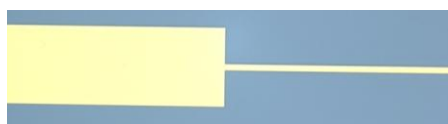


Figure 19. Optical microscopy image of Au electrodes after metal lift-off in positive resist stripper PRS 2000 at RT for 1 h.

penetration of the resist stripper. The resist was completely removed and the edges were not contaminated, as shown in Figure 19. The PRS is a strong resist remover. In order to avoid damage to the electrodes the wafers have to be dipped very gently into DI water to wash off the PRS. When rinsing with DI water especially small electrodes are removed from the wafer due to low adhesion.

Embedding of the bottom electrodes in optical adhesive and applying of supports

For template-stripping mechanical supports are needed. Therefore, glass slides (1.2x1.8 cm²) are used for the bottom electrodes. In order to avoid contaminations the glass is cleaned with piranha solution (3:1 → sulfuric acid (H₂SO₄) : hydrogen peroxide (H₂O₂)) for 30 min. After piranha cleaning the glass slides are washed two times in Milli-Q water, rinsed with ethanol and dried with N₂.

The optical adhesive (OA, Norland) which is used to glue the glass slides to the electrodes sticks strongly to silicon. To lower the adhesion between the OA and the Si wafer, an anti-sticking layer is formed. Therefore, 0.05 ml of 1H, 1H, 2H, 2H-perfluorodecyl-trichlorosilane (PFDTs) is placed in a desiccator together with the Au patterned wafers. The desiccator is pumped down for 10 min. The wafers are fluorinated by gas phase deposition of the PFDTs for 60 minutes. The glass slides are applied above the electrodes with a droplet of OA. After applying of the supports, the OA is cured under UV light for two hours.

Template-stripping of bottom electrodes

The glass supports with the OA/Au are template-stripped from the wafer by moving a scalpel blade between the OA and the wafer. The metal electrodes stick better to the OA than to the silicon wafer and are separated from the wafer during template-stripping^{16,31}. The flipped electrodes are ultra-smooth because their roughness is a copy of the silicon wafer surface.

The different steps of the metal electrode fabrication are summarized in Figure 20.

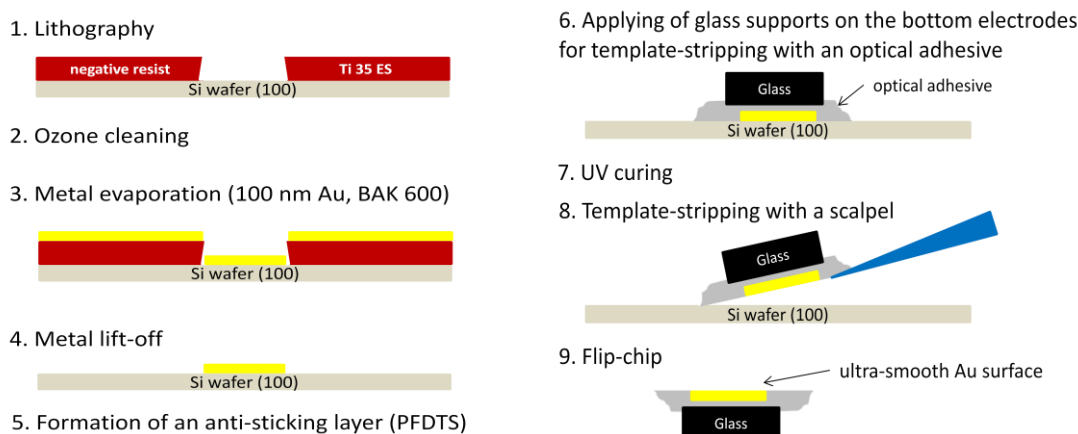


Figure 20. Fabrication steps for template-stripped Au electrodes.

Molecular layer formation

The monolayers of decanethiol (C_{10}), dodecanethiol (C_{12}), tetradecanethiols (C_{14}), hexadecanethiols (C_{16}) and octadecanethiols (C_{18}) were respectively formed on the bottom metal electrodes by immersing the freshly template-stripped electrodes overnight (around 18 hours) into a 5 mM ethanolic solution of the thiols. The solution is kept under argon atmosphere. After thiol formation the electrodes are gently rinsed with ethanol and dried with N_2 .

Applying of the top electrodes

- Top electrodes on a PDMS stamp

In order to prevent damaging the SAM formed on the bottom electrodes it is of crucial importance to softly apply the top electrode. Therefore, many attempts were performed to place the top electrode. In the original flip-chip concept the top electrodes were also template-stripped. As support a PDMS stamp was used and glued to the Au electrodes with an OA. The top electrodes on the PDMS stamp were held with tweezers and placed by hand on the bottom electrode and gently pressed to make contact. Most of the measured junctions were shorted, which is most probably due to the fact that too much pressure is applied. Another problem was trapped air in between the junction which gave open circuits. Therefore a droplet of fluid was placed on the monolayer and the top electrode was placed above it. Both water and ethanol were used as fluid. The top electrode was softly lowered to the monolayer by evaporation of the liquid in a desiccator overnight. Hereby the electrodes gently make contact without application of force. Although the contacting of the top electrode should be softer the yield did not increase.

- Soft landing of top electrodes via wedging transfer

A softer way to apply micro- and nanostructures is wedging transfer. Hereby the top electrodes on the wafer were dipped for 5 sec into cellulose acetate butyrate (30 mg/ml) in ethyl acetate including 0.1 volume % of 1-dodecanethiols to enhance the sticking of the polymer to the gold. The polymer was dried under ambient conditions for 3 minutes. In order to allow a good wedging transfer the polymer is dissolved at the bottom side and at the edges of the wafer with ethyl acetate so that only the part with the electrodes is covered. The wafer is then slowly dipped into Milli-Q water under an angle of about 70° . This angle allows the lift-off of the polymer from the wafer. In the case that the

angle is too flat or too steep the water does not penetrate at the interface. The cellulose acetate butyrate film including the gold electrodes lifts off from the wafer and floats on the water. This is due to the fact that water penetrates at the interface between the hydrophilic and the hydrophobic surfaces. The polymer is hydrophobic, while the Si wafer after treatment with the PRS is hydrophilic. Gold electrodes which were fabricated with metal lift-off in PRS 2000 did not need any further processing before wedging transfer. Even after storing for 5 days under ambient conditions wedging transfer gave the same results. Electrodes fabricated with metal lift-off in acetone were treated with 20 sec plasma oxidation before wedging transfer. With plasma oxidation or UV-ozone cleaning it was also possible to transfer the electrodes from the wafer after 5 days of storage. Without plasma oxidation it is not possible to transfer the electrodes. The difference between samples fabricated with lift-off in PRS 2000 and acetone is due the hydrophilicity of the silicon substrate. The contact angle of a wafer that had been in PRS 2000 is $27.8^\circ \pm 1.1^\circ$ which indicates a hydrophilic surface. In comparison the contact angle measured for a wafer after lift-off in acetone is 60.1 ± 0.4 . The contact angle is much higher and therefore wedging transfer is not possible. Plasma oxidation and UV-ozone treatment enhance the hydrophilicity. Optical microscope images showed no damage due to plasma and UV-ozone treatments to the gold electrodes. But in order to exclude any influence of the extra step to the electrodes, samples lifted-off in PRS are used for the fabrication of molecular junctions.

For an exact alignment of the top electrodes on the bottom electrodes covered with the monolayer a special setup was made. A photograph is shown in Figure 21. The bottom electrodes are at the bottom of the glass beaker filled with Milli-Q water. At the surface of the water the top electrodes are floating. The top electrodes embedded in the cellulose acetate butyrate are held with a micromanipulator while the water level is slowly decreased by a syringe pump. This technique allows a gentle landing of the top contact and minimizes the creating of shorts. After contact is made the molecular junction device is placed in a desiccator overnight to evaporate the water between the top and bottom contacts.

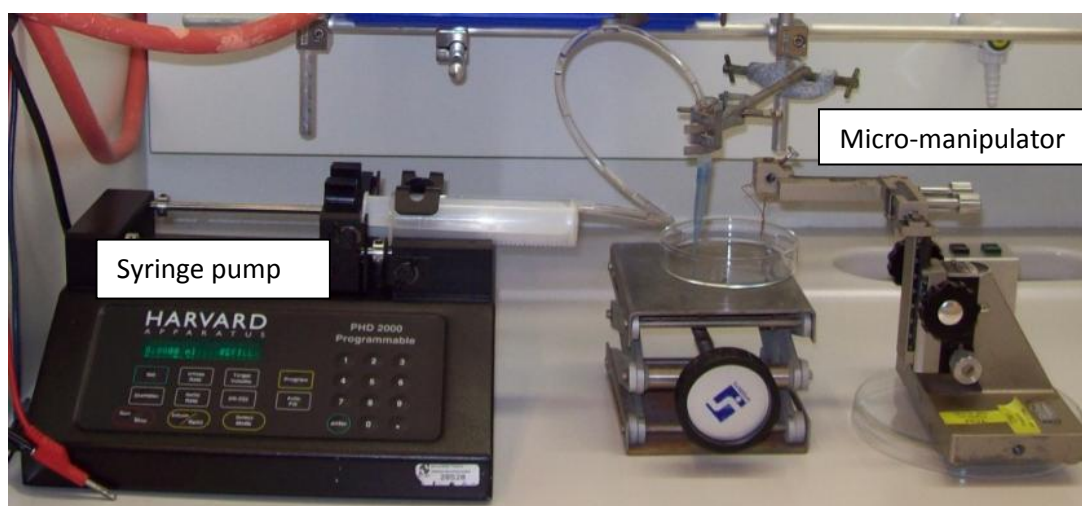


Figure 21. Set-up for wedging transfer; the cellulose acetate butyrate film with the Au contacts is floating on water in the glass beaker (middle) and it is aligned with a micromanipulator (right), contact with the bottom electrodes with the monolayer is made by slowly lowering the water level by pumping out the water with a syringe pump (left).

A schematic picture of the molecular junction fabrication with wedging transfer is shown in Figure 22.

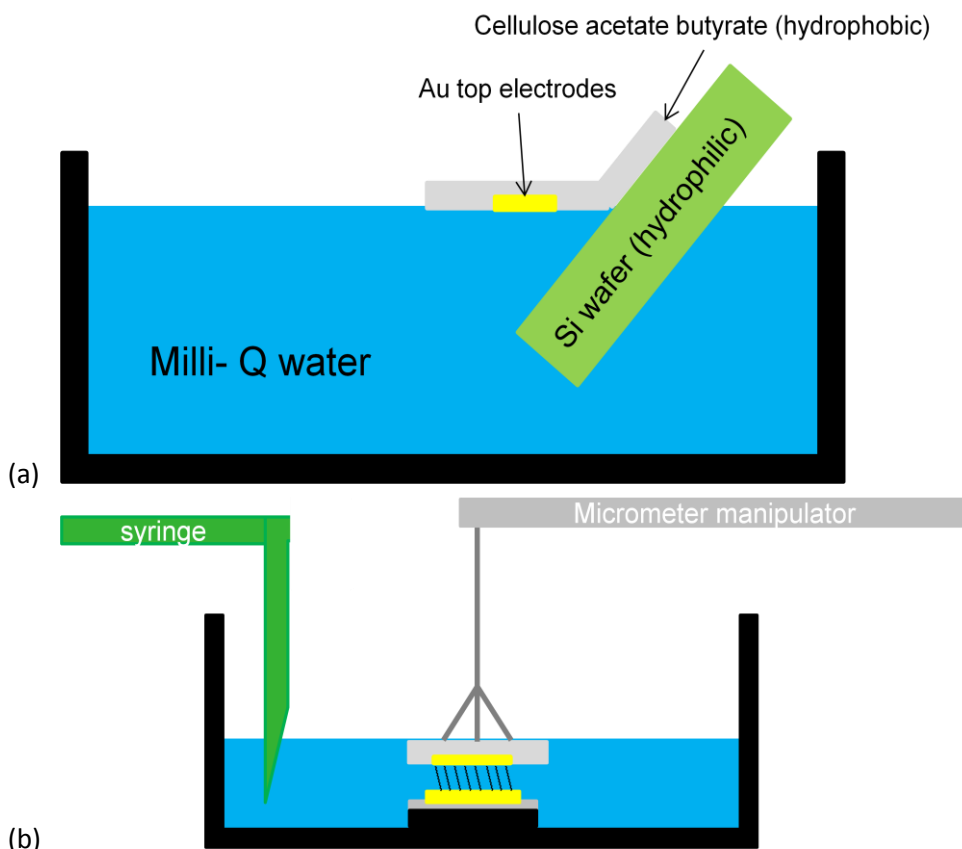


Figure 22. Illustration of wedging transfer; (a) the hydrophobic polymer film including the Au electrodes is lifted-off from the hydrophilic wafer, (b) bottom electrodes covered with SAMs are placed at the bottom of the glass beaker and the polymer film is aligned with a micromanipulator on top of the monolayer while the water is slowly pumped out with a syringe pump.

3.3. Analysis of the metal electrodes

For the metal electrodes gold (Au), silver (Ag) and platinum (Pt) were investigated. The platinum electrodes showed a surface with fractures over the whole device after metal lift-off. Also an evaporated Pt layer over a non-pattered wafer showed these cracks. An optical microscope image of platinum electrodes is shown in Figure 23. Due to the damages platinum electrodes were not further studied.

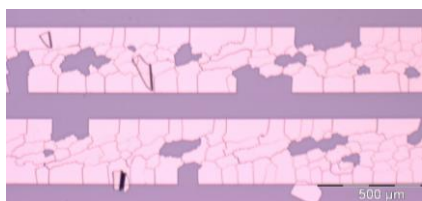


Figure 23. Optical microscope image of Pt electrodes after metal lift-off in acetone.

The surfaces of the silver and gold bottom electrodes were analyzed with atomic force microscopy (AFM) in tapping mode. The interface between the optical adhesive and the metal electrodes as well as the surface root-mean-squared (rms) roughness were examined.

Template-stripping worked well for both materials. But silver electrodes had a higher surface roughness than Au which might be due to oxidation after template-stripping. The rms roughness in the middle of template-stripped Ag electrodes was 6 nm. The surface rms roughness of the gold electrodes was below 0.5 nm. The rms roughness was

measured over an area of $2 \times 2 \mu\text{m}^2$. Due to their low roughness all further electrodes were fabricated with Au. The AFM images of template-stripped Ag and Au electrodes are shown in Figure 24.

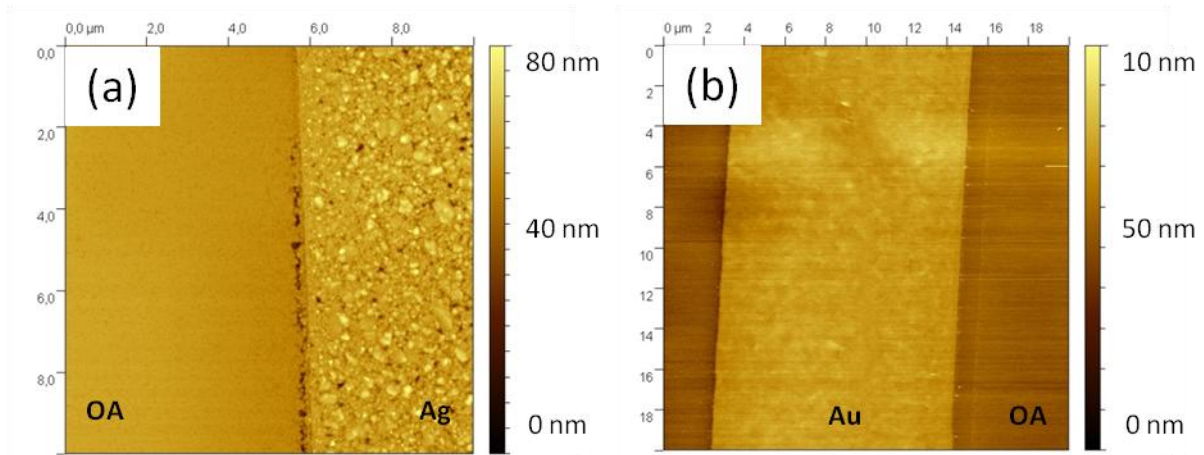


Figure 24. (a) AFM image of the interface between the OA and a silver electrode after template-stripping; the rms roughness of the Ag electrode is 6 nm ($2 \times 2 \mu\text{m}^2$); (b) AFM image of a $10 \mu\text{m}$ Au electrode after template-stripping embedded in OA; the rms roughness is 0.33 nm ($2 \times 2 \mu\text{m}^2$).

AFM analysis showed that there was a gap at the OA/electrode interface. This was observed for Au as well as for Ag. The edges were not symmetrical on both sides of the electrodes and showed two different geometries. One edge was sharp and had a deep narrow gap between the metal and the optical adhesive (Figure 25). The other edge showed a smoother interface between the electrode and the optical adhesive. It was considered that this might come from the metal evaporation. The wafers are normally placed in rotating holders which are under an angle directional to the metal source. Therefore a special fixed holder was utilized to exclude the influence of different angles. The AFM imaging showed the same geometries for evaporation in both sample holders, which means this is not caused by the metal evaporation process.

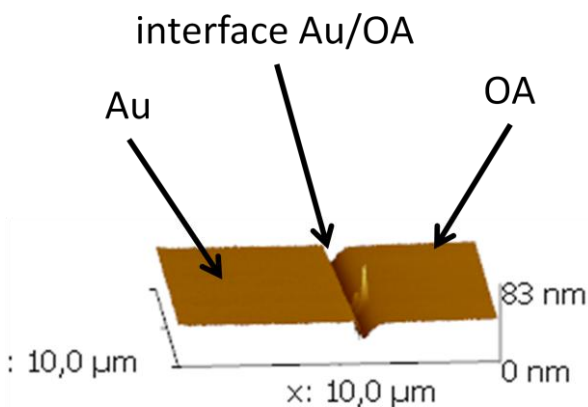


Figure 25. AFM image of the Au/OA interface after template-stripping.

The first conclusion was that the gap between the OA and the metal might be caused during template-stripping. Therefore, electrodes were template-stripped from two different sides and afterwards compared with AFM. They showed the gap on the same side of the electrode thus the direction of template-stripping has no influence on the interface between the OA and the electrodes.

The deep narrow gap between the OA and the electrodes was already observed earlier. The researchers supposed that this effect is caused by shrinkage during the polymerization of the optical adhesive¹⁶.

By looking at the height differences between the OA and the Au electrodes it was observed that the electrodes were protruding up to 10 nm from the OA like shown in Figure 26.

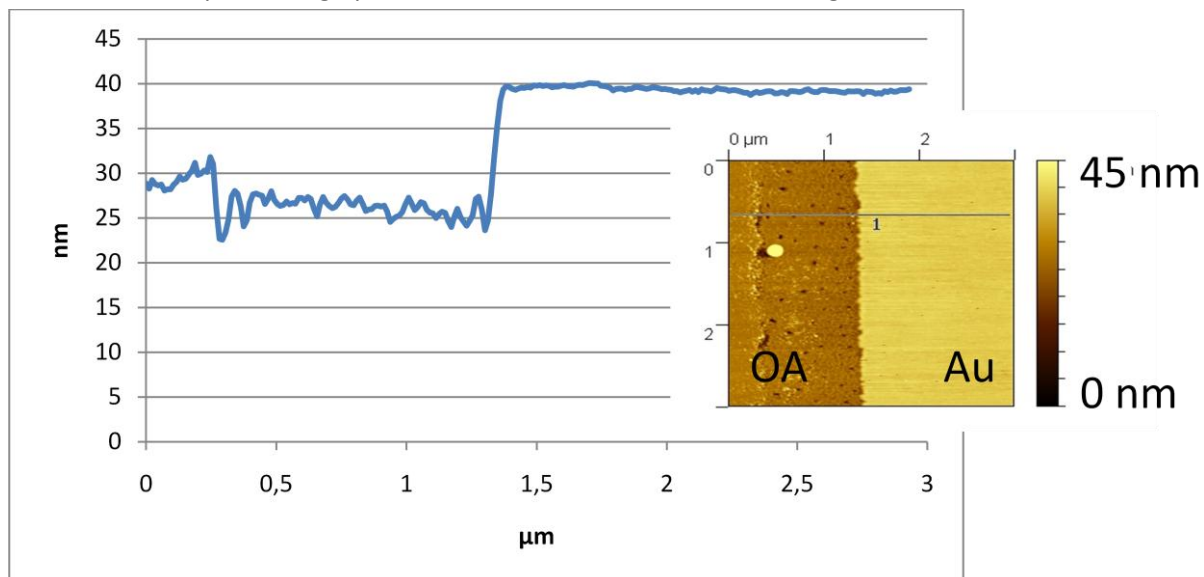


Figure 26. Cross-section of the interface between OA and Au after template-stripping; the protrusion of the Au electrode is >10 nm.

The protrusion might be the reason why often shorts were measured for the molecular junctions. Therefore it was tried to remove the protrusions. Freshly template-stripped gold electrodes were etched. The gold etch solution consisted of KOH (1402.8 mg), $\text{Na}_2\text{S}_2\text{O}_3$ (620.5 mg), $\text{K}_3\text{Fe}(\text{CN})_6$ (82.4 mg) and $\text{K}_4\text{Fe}(\text{CN})_6$ (10.6 mg) in 25 ml Milli-Q water. The etch rate of this solution is 3 nm/min. The samples were etched for 3 minutes in order to achieve a lower protrusion. It was not possible to overcome the protrusions with this etch solution.

AFM images showed that the rms roughness of the Au surface increased as expected, but that the optical adhesive was unexpectedly also etched (Figure 27). The step at the OA/Au interface increased in the order of several nanometers.

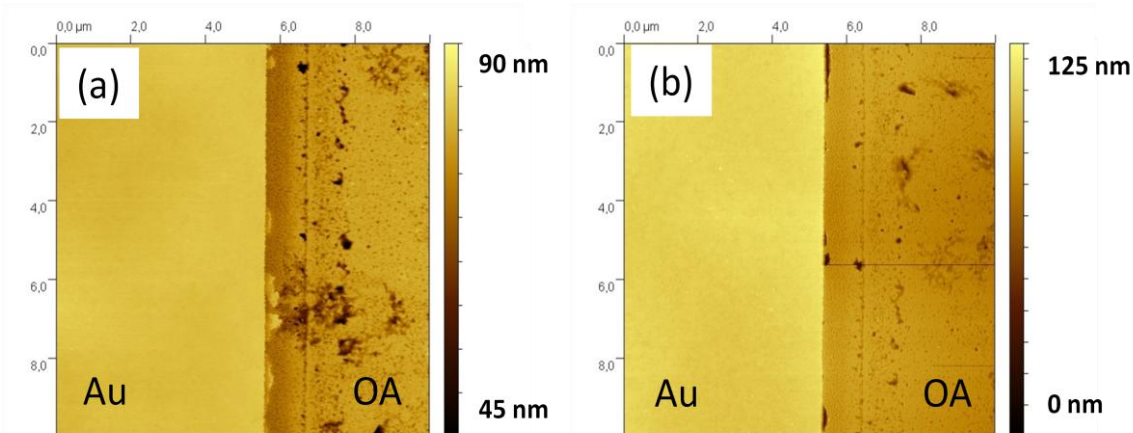
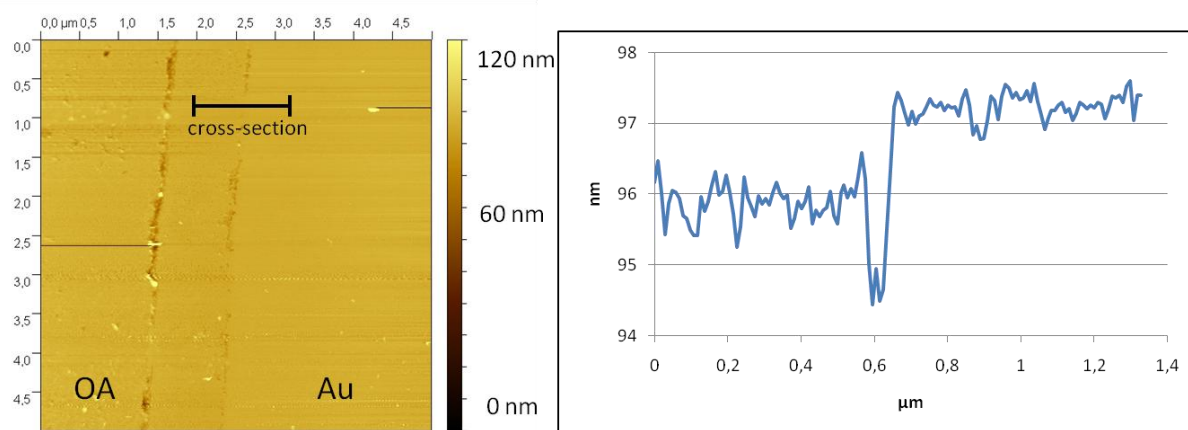


Figure 27. AFM images of the OA/Au interface before (a) and after (b) 3 min Au etch; the Au electrode protrusion increased from 5 nm before etching to 17 nm after etching, also the rms roughness increased from 0.47 nm before to 1.7 nm after etching.

Another fabrication technique was tried to get less protrusions of the electrodes. The electrodes were embedded in poly (methyl methacrylate) (PMMA) instead of optical adhesive. An anti-sticking layer was formed before spin-coating of the PMMA. The PMMA with a molecular weight of 350 kD (6 wt% in toluene) was spin-coated first at 500 rpm (5 sec) followed by 3000 rpm 30 (sec) and then baked for 1 min at 120°C. Subsequently the OA is applied to glue the glass slide to the Au/PMMA. In order to enhance the contact between the OA and PMMA plasma oxidation of the PMMA was done for 20 sec. Then the OA was UV-cured for 2 hours. Template-stripping was possible with these devices. The template-stripped electrodes were analyzed with AFM. The electrodes were less protruding from the PMMA compared to Au/OA devices. The protrusion was between 1 and 2.5 nm. Two AFM images and the corresponding cross-section at the interface between PMMA and Au are shown in Figure 28.

(a)



(b)

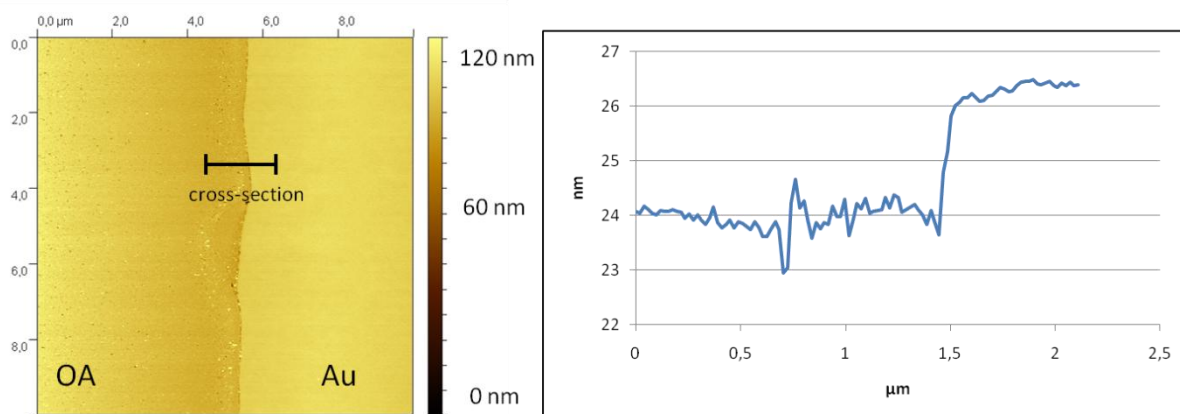


Figure 28. AFM images of template-stripped Au electrodes embedded in PMMA; the protrusion of the Au electrodes are 1 nm (a) and 2.5 nm (b).

These devices looked very promising but when immersing the template-stripped electrodes into an ethanolic thiol solution the PMMA swelled up making it impossible to apply the top electrode to form molecular junctions. An image of electrodes after storage overnight in ethanol is shown in Figure 29.

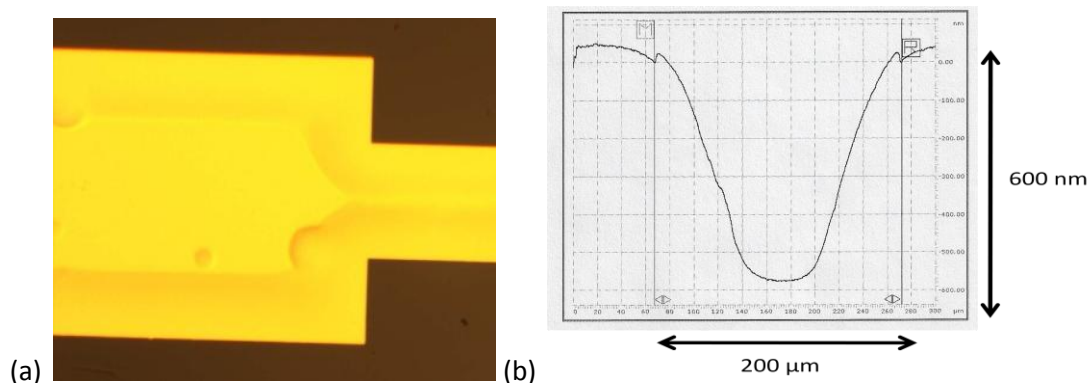


Figure 29. (a) Optical microscope image of a template-stripped Au electrode embedded in PMMA after storage in ethanol overnight; PMMA is swelling in ethanol, (b) Dektak topograph of the template-stripped 200 μm Au electrode, the swelling of the PMMA causes a deformation of the electrode.



Figure 30. Optical microscope image of a template-stripped Au electrode embedded in PMMA; the PMMA was cooled down slowly after spin-coating and baking at 120°C and the UV-curing time was reduced.

Further experiments have to be done to form molecular junctions with template-stripped Au/PMMA bottom electrodes. Approaches were already made by cooling down the PMMA very slowly after heating at 120°C and reducing the time for UV-curing of the OA from 2 hours to 30 min. From optical microscope images no conclusion could be drawn (Figure 30). The images show no swelling of the PMMA but it might also be possible that the whole electrode is elevated. Further investigations have to be done on PMMA to see if the swelling could be controlled or even prevented because the small protrusions might allow higher working device yields for the flip-chip concept.

3.4. Characterization of the SAMs

The quality of the SAMs was measured with advancing θ_a and receding θ_r water contact angle (CA) in air. The hysteresis between the advancing and receding CA is shown in Table 4 for the different kinds of alkanethiols.

Table 4. Water contact angle and hysteresis for C_{10} , C_{12} , C_{14} , C_{16} and C_{18} .

Alkanethiol (# of carbon atoms)	Contact angle ($^\circ$)	Advancing CA	Receding CA	Hysteresis [$\theta_a - \theta_r$] ($^\circ$)
C_{10}	106.73 ± 0.95	103.45 ± 0.33	74.16 ± 0.21	29.29
C_{12}	104.5 ± 0.6	104.58 ± 0.63	86.67 ± 0.44	17.92
C_{14}	101.1 ± 1.6	103.97 ± 0.19	87.71 ± 0.16	16.26
C_{16}	111.5 ± 1.2	112.77 ± 0.08	98.41 ± 0.24	14.36
C_{18}	102.0 ± 2.9	106.69	92.59	14.1

A good quality SAM of alkanethiols with chain lengths of 10 or more carbon atoms is characterized by a contact angle of about $111^\circ - 114^\circ$ ³⁴. The angle hysteresis for alkanethiols on polycrystalline surfaces is known to be between 10° and 20° ⁶. The contact angle of the hexadecanethiols (C_{16}) was better than the ones measured for the other SAMs. Lower contact angles as well as a large hysteresis

indicate defects in the monolayer, which influence the yield and spread in current densities of the molecular junctions.

Nuclear magnetic resonance (NMR) spectroscopy was used in addition to investigate the purity of the alkanethiols. The spectra showed no additional peaks caused by possible contaminations. The purity of the alkanethiols is important for a high quality of the SAM.

4. Electrical measurements

The molecular junctions have a cross-bar structure with junction areas originally between 10×10 and $200 \times 200 \mu\text{m}^2$. A new mask was designed because it turned out that smaller junctions gave higher

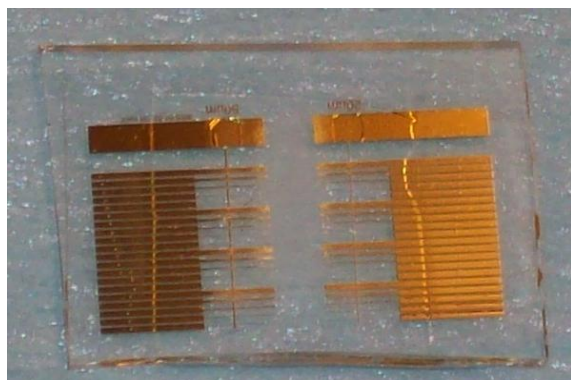


Figure 31. Photograph of a sample with 20 molecular junctions on each side; the top electrode is applied via wedging transfer.

working device yields and lower spread in current density. The new contact areas were between 10×10 and $50 \times 50 \mu\text{m}^2$. The design is such that the contact pads are far away from the junctions, limiting damage to the junctions. It also made characterization with a standard probe station possible. A picture of one sample is shown in Figure 31. On each sample there are 40 junctions scaling between 10 and 50 μm for the top and bottom electrodes.

The electrical measurements were done with a Karl Süss probe station connected to a Keithley 4200 Semiconductor Characterization System.

The current-voltage curves were measured by varying the applied voltage in steps of 5 mV from 0 V to 1V, then from 1V to -1V and back to 0V. Each measurement hence had 804 data points. The applied voltage was started at 0V to avoid rapid voltage changes across the molecular junction. The I - V curves were not reproducible when the applied voltage was started directly at 1V.

In the case that the current is transported through the monolayer a non-linear I - V curve is measured. If the molecular junction is shorted, which means that there is a direct contact between the bottom and top electrode, a linear ohmic I - V curve is measured. The measured resistance is several $\text{M}\Omega$. For the opposite case that the two electrodes are not contacted an open circuit characterized by noisy I - V curves with resistances in the $10^{15} \Omega$ region is monitored. These resistance values are the current noise level of the setup.

A working molecular junction is characterized by a non-linear I - V slope with currents below 10^{-3} A ($\sim \text{G}\Omega$). In this thesis a working molecular junction is defined as followed. Each junction must be measureable for at least 10 times and the current of these 10 measurements has to be reproducible which means that the spread in current should be below a factor of three. The current densities for the alkanethiols with different chain lengths are calculated by averaging the $\log|J|$ of the ten measurements for each junction. In each I - V measurement the current is measured two times for a given voltage. The difference in current values of these two sweep directions is negligible. These logarithmic current densities are then averaged for one type of alkanethiol (C_{10} - C_{18}) and calculated back to current density, $10^{\log|J|}$. The standard deviation is also calculated over the averaged $\log|J|$. Due to our large standard deviation, the ± 1 standard deviation is not shown in the J - V graphs. Therefore, the ± 1 standard deviation is given in the graphs showing the current density at a given voltage as a function of the thickness of the SAM. The average current density and standard deviation are calculated with the $\log|J|$ because the current density is exponentially dependent on parameters like for example the SAM thickness. Due to the SAM thickness dependence of J , the current densities can vary orders of magnitude. A log-normal distribution of current density has been reported by Whitesides *et al*⁹. By taking the average directly over the J the average J is highly biased towards higher J . An example of the biasing to higher voltages is given in Figure 32.

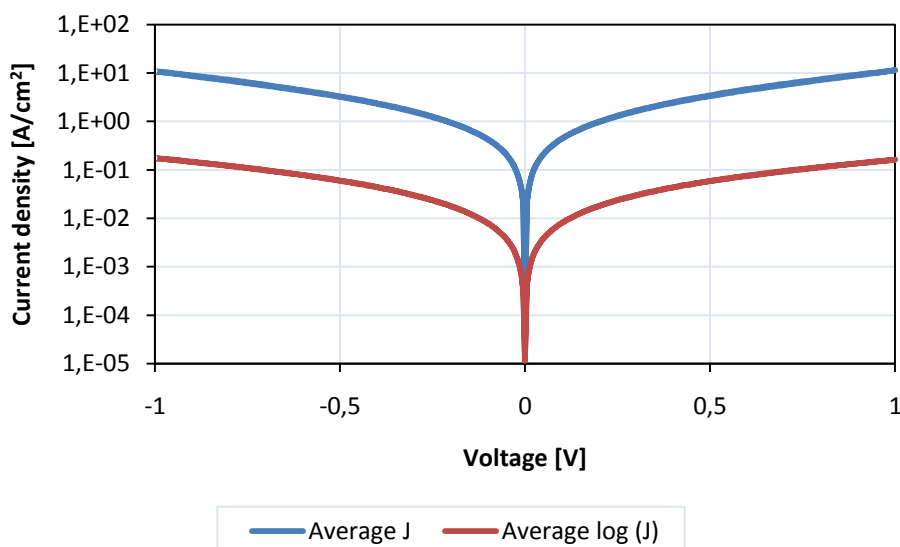


Figure 32. Averaged J - V plots of Au-C₁₂-Au molecular junctions; the contact areas are between 100 and 400 μm^2 . The averaged J was calculated by directly taking the average over J and by averaging the $\log(J)$ respectively.

4.1. Experimental results

The working device yields and the current densities for different techniques for applying of the top electrodes are discussed below.

The original flip-chip concept gave a working device yield of $\sim 10\%$ and a spread in current density of six to seven orders of magnitude¹¹. In the beginning of the project the original flip-chip concept was repeated. This means that the top electrodes were template-stripped with a PDMS support and placed with tweezers on top of the monolayer. With this small batch an even lower yield of 1.7% was achieved. To improve the overall yield, it was tried to attain a softer landing by placing a DI water and ethanol droplet respectively between the top and bottom contacts. The liquid was evaporated in a desiccator overnight allowing the top electrode to gently make contact with the molecules. Although this should be a softer landing the yield did not increase (see Table 5). The molecular junctions were categorized in four groups. “Later shorted” means that the junction was shorted before 10 sequenced measurements were done.

Table 5. Working device yields of molecular junctions fabricated with the original flip-chip concept as well as flip-chip junctions with a water and ethanol droplet between the contacts.

Sample [# of measured junctions]	Shorted [%]	Later shorted [%]	Open circuits [%]	Working devices [%]
Flip-chip [120]	62.5	2.5	33.3	1.7
Flip-chip with water droplet [80]	61.3	3.7	35	0
Flip-chip with ethanol droplet [40]			100	0

As described before, the electrodes were etched, resulting in even higher steps between the metal and the optical adhesive as well as a higher rms roughness of the Au electrode surfaces. However, molecular junctions were fabricated because the etching process might have removed the sharp features at the Au electrodes which then would allow a better monolayer formation at rounded edges. The working device yields are shown in Table 6.

Table 6. Working device yields of molecular junctions with etched electrodes.

Sample [# of measured junctions]	Shorted [%]	Later shorted [%]	Open circuits [%]	Working devices [%]
Flip-chip [40]			100	0
Flip-chip with water droplet [237]	37.5	10.5	40.5	11.5

The yields were slightly higher than compared to the molecular junctions before, but the spread in current densities of seven orders of magnitude was too large to draw any reliable conclusions concerning the transport behavior of different alkanethiols. Furthermore, the curves were often characterized by large offsets at zero voltage. These offsets most probably indicate that the contact between the molecules and the top electrode is not good as offsets are also observed for open circuits. The Au electrodes were etched after template-stripping for 2 minutes with an etch solution based on KOH, $\text{Na}_2\text{S}_2\text{O}_3$, $\text{K}_3\text{Fe}(\text{CN})_6$, $\text{K}_4\text{Fe}(\text{CN})_6$ and water. The etch rate was 3 nm/min. The monolayer was formed on the etched bottom electrodes and the top contact was applied with a water droplet above the molecules. The device was placed in a desiccator overnight to remove the water. The observed offsets might be due to remaining water between the contacts. Remaining water might inhibit a good contact of the top electrode with the molecules. Due to the large spread in J and the shifted current densities, Au etch was not the method of choice to improve the flip-chip concept.

A reason for the large spread in J and the low yield might be too rough application of the top electrode. It is possible that the monolayer is damaged by placing the top contact by hand above the SAMs. Therefore, wedging transfer³², which should give a softer landing, was tried. The bottom electrodes were fabricated with the original flip-chip concept which means template-stripping from a Si wafer.

The working device yields for the molecular junctions fabricated with alkanethiols of different chain lengths are shown in Table 7 and Table 8.

Table 7. Working device yields for C_{10} – C_{18} alkanethiols fabricated with wedging transfer for junction areas between 10×10 and $50 \times 200 \mu\text{m}^2$.

Alkanethiol [# all junctions]	Shorted [%]	Later shorted [%]	Open circuits [%]	Working devices [%]
C_{10} [78]	53.8	6.4	2.6	37.2
C_{12} [118]	51.7	10.2	0.8	37.3
C_{14} [101]	42.7	1.9	3.9	51.5
C_{16} [113]	68.1	2.7	6.2	23.0
C_{18} [115]	58.3	8.7	3.5	29.5

Table 8. Working device yields for C_{10} – C_{18} alkanethiols fabricated with wedging transfer for junction areas between 10×10 and $20 \times 20 \mu\text{m}^2$.

Alkanethiol [# only 10 and 20 μm]	Shorted [%]	Later shorted [%]	Open circuits [%]	Working devices [%]
C_{10} [24]	16.6	4.2	12.5	66.7
C_{12} [32]	46.8	12.5	6.3	34.4
C_{14} [34]	44.1	0	5.9	50.0
C_{16} [22]	49.9	0	13.6	45.5
C_{18} [39]	61.5	15.4	5.1	18

The working device yield increased significantly for molecular junctions fabricated with wedging transfer. Therefore, this application technique was used for the electrical characterization of monolayers. It was observed that the working device yield was higher for nearly all chain lengths if the junction area was smaller. The working device yield was between 18% and 67% for junction areas up to $400 \mu\text{m}^2$ and between 23% and 52% for junction areas up to $10,000 \mu\text{m}^2$. This is a huge improvement compared to direct evaporation of the top contact with a yield of $\sim 1\%$ ⁸. However, the yield is not as high as the yields for molecular junctions based on alkanethiols fabricated with a conductive polymer film (PEDOT:PSS) on top of the monolayers ($> 95\%$)¹⁰, EGaIn ($\sim 80\%$)⁹ or graphene as top electrode ($\sim 90\%$)³⁰. An advantage of the flip-chip concept over these techniques is that the top and bottom contacts are the same metal which overcomes ambiguities that appear when an additional layer is introduced between the SAM and the top contact. The origin of the large spread in J could be called a disadvantage of our technique. However, we are not sure what the origin is. Leaving the molecular junctions overnight in a desiccator is maybe not enough to remove all water from inside the junction. Measuring under vacuum can probably overcome this problem. By looking at Table 3 one can see that also for EGaIn and graphene based molecular junctions the spread is quite large with up to 2 orders of magnitude for C_{14} . The lowest spread was reported for molecular junctions with PEDOT:PSS-based molecular junctions.

The working device yield for our flip-chip molecular junctions increased with decreasing junction area. This is most probably due to the higher possibility of defects in the monolayer for larger contact areas. The J - V characteristics and current densities at 1V of C_{10} , C_{12} , C_{14} , C_{16} and C_{18} for junction areas between $10,000$ and $100 \mu\text{m}^2$ versus the chain length of the alkanethiols are shown in Figure 33 and Figure 34, respectively. The current density is expected to decrease with increasing chain length of the SAM, resulting in an exponential relationship between J and the number of carbon atoms in the alkanethiol chain. For the large contact areas J of octadecanethiols (C_{18}) was found to be higher than for hexadecanethiols (C_{16}) and the error bars were large with 1.5 orders of magnitude. The log-standard deviation for decanethiols (C_{10}) was also very large and J was lower than for dodecanethiols (C_{12}). This does not allow reliable analysis of the dependence of J on the length of the SAMs.

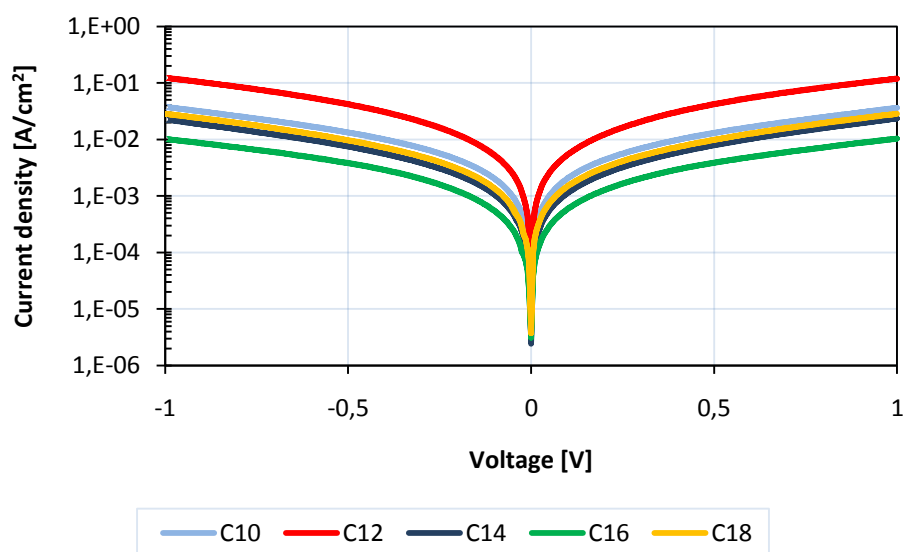


Figure 33. Comparison of the J - V characteristics of C_{10} , C_{12} , C_{14} , C_{16} and C_{18} alkanethiols with contact areas between 100 and $10,000 \mu\text{m}^2$.

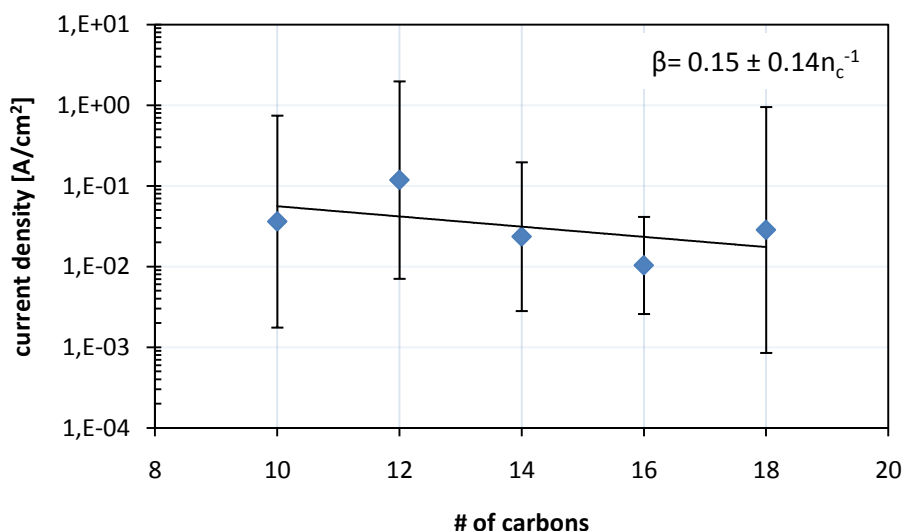


Figure 34. Plot of the current densities at 1V with +/- 1 standard deviation as a function of the chain length of alkanethiols; the tunneling decay coefficient β [n_c^{-1}] is determined to be 0.15 ± 0.14 . The contact areas are between 100 and 10,000 μm^2 ; the solid line expresses an exponential fit through the data points.

The least squares fit through the data points in Figure 34 shows a slight exponential dependence of J on the chain length of the alkanethiols. The error of the β coefficient was determined with a built-in algorithm of the data analysis software Origin. As the current density obeys the equation $J = J_0 e^{-\beta d}$, the tunneling decay coefficient β can be determined from the slope of the fit. The β coefficient gives information about the transport mechanism through the molecular junction. The exponential length dependence in the equation given above is valid for direct tunneling through short molecules (< 3 nm) such as alkanethiols. For longer molecules a transition from tunneling to hopping occurs, which scales linearly¹⁸. Hopping transport conductance is characterized by weak inverse length dependence¹⁹.

An exponential dependence of J on the molecular chain length of the alkanethiols confirms that the measured currents are characteristic for the different thicknesses of the SAMs¹⁰ (see paragraph about "Transport behavior of Alkanethiols"). For large junction areas the β coefficient has a value of $0.15 \pm 0.14 n_c^{-1}$. Due to this very low β value as well as the huge error bars no meaningful conclusions can be drawn for the measured current densities as a function of the SAM thickness when the molecular junction areas are up to 10,000 μm^2 large.

Figure 35 shows the J - V characteristics and Figure 36 shows current densities at 1V of C_{10} , C_{12} , C_{14} , C_{16} and C_{18} for junction areas between 100 and 400 μm^2 for different chain length of the alkanethiols. The current density decreases exponentially with the SAM thickness. The β coefficient is determined to be $0.45 \pm 0.10 n_c^{-1}$. The J value for C_{18} is lower than for C_{16} but the J value for C_{10} is also for smaller junctions not higher than for C_{12} .

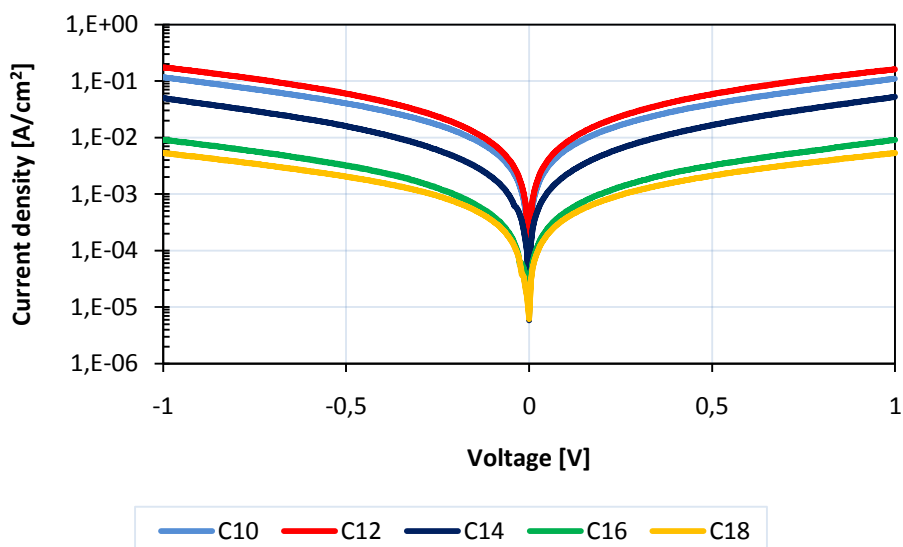


Figure 35. Comparison of the J - V characteristics of C_{10} , C_{12} , C_{14} , C_{16} and C_{18} alkanethiols with contact areas between 100 and 400 μm^2 .

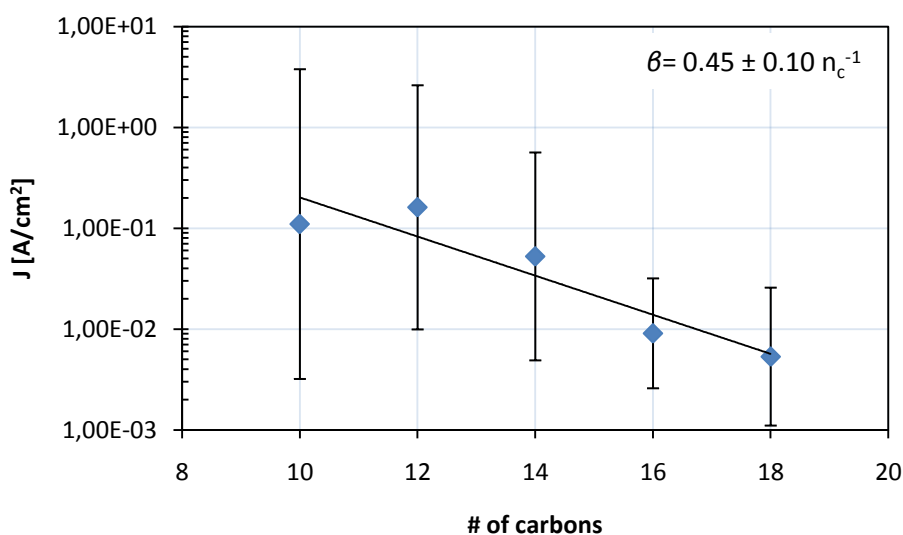


Figure 36. Plot of the current densities at 1V with ± 1 standard deviation as a function of the chain length of alkanethiols; the tunneling decay coefficient θ [n_c^{-1}] is determined to be 0.45 ± 0.10 . The contact areas are between 100 and 400 μm^2 .

Therefore, the electrical characterization of the SAMs was done with smaller junction areas between 100 and 400 μm^2 . Decanethiols (C_{10}) were not included into the analysis because they also showed a large spread in current densities for small junctions and the J values were lower than the ones for dodecanethiols (C_{12}). A reason might be defects in the monolayer indicated by a large hysteresis for advancing and receding contact angle (see Table 4). We therefore decide to study the behavior leaving out the C_{10} results. The J - V curves for small junctions with C_{12} , C_{14} , C_{16} and C_{18} are presented in Figure 37. Current densities of alkane-monothiol reported in literature differ up to eight orders of magnitude for different fabrication techniques (see Table 2). The J values measured with the combination of the flip-chip concept and wedging transfer were found to be about in the middle of the reported current densities.

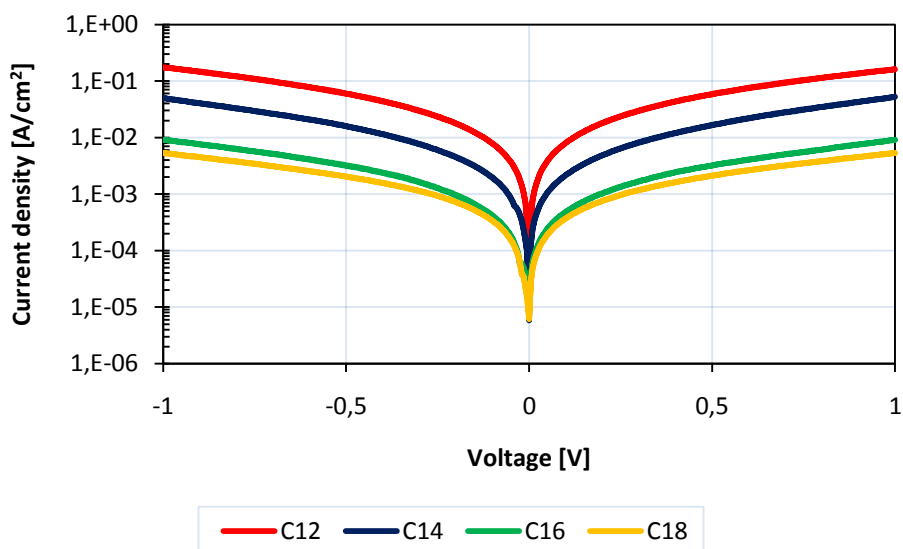


Figure 37. Comparison of the J - V characteristics of C_{12} , C_{14} , C_{16} and C_{18} alkanethiols with contact areas between 100 and 400 μm^2 .

In Figure 38 the current densities at 1V are plotted as a function of the molecular length. The error bars represent ± 1 standard deviation. For small junction areas and alkanethiols from C_{12} to C_{18} the β coefficient was measured to be 0.60 ± 0.11 per carbon atom showing that the measured current density depends on the lengths of the alkanethiols. By comparing the value with reported β coefficients in literature, our decay coefficient is lower. The tunneling decay coefficients for alkanethiols are reported to be around 1 n_c^{-1} (see Table 1)^{9,16,29,30}. As the application of the top electrodes is water-based, the high standard deviation might originate from trapped water. Trapped water would mean a less perfect contact between the SAM and the top electrode. If this is the case the trapped water affects J and consequently J is not completely dominated by the length of the alkanethiols.

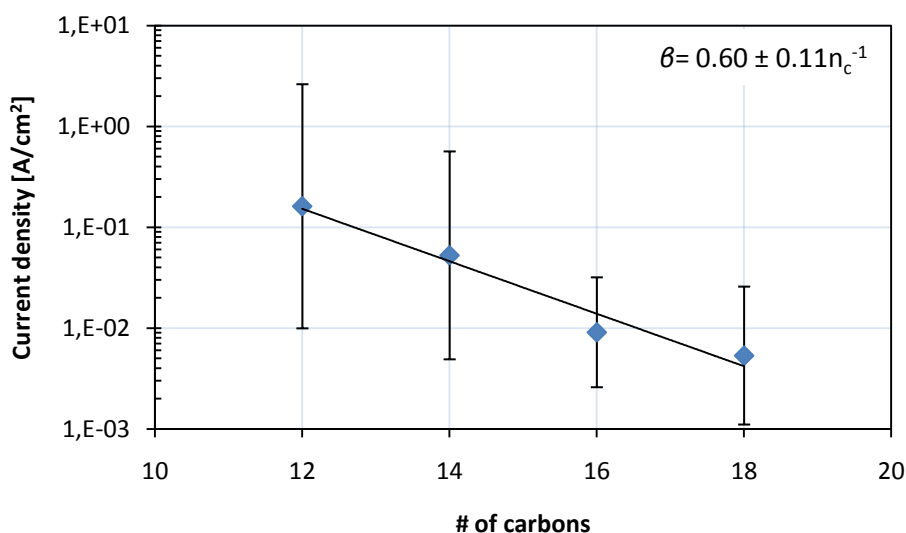


Figure 38. Plot of the current densities at 1 V ± 1 standard deviation as a function of the chain length of alkanethiols; the tunneling decay coefficient β [n_c^{-1}] is determined to be 0.60 ± 0.11 . The contact areas are between 100 and 400 μm^2 .

As the β coefficients in literature are generally reported for 0.2V, 0.5 V or 1V, the tunneling decay coefficient of our molecular junctions was also calculated at 0.2V and 0.5 V. The β values were $0.55 \pm 0.10 n_c^{-1}$ at 0.2V and $0.58 \pm 0.09 n_c^{-1}$ at 0.5V. These values are nearly equal to the β coefficient at 1V (see Figure 39).

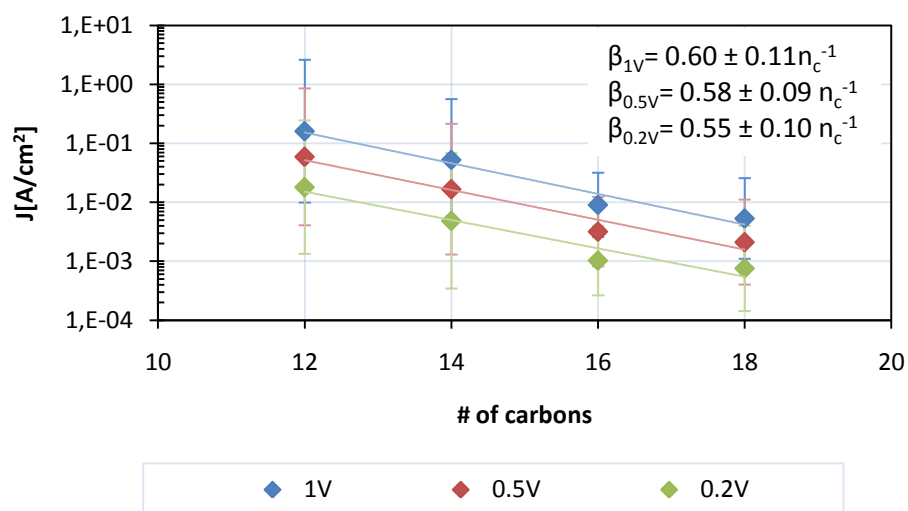


Figure 39. J values measured at 0.2V, 0.5 V and 1 V as a function of the chain length of the alkanethiols with +/- 1 standard deviation.

Figure 40 shows the current density as a function of SAM thickness at 0.2V, -0.2V, 0.5V, -0.5V, 1V and -1V. As expected there are no differences in J between positive and negative applied voltages.

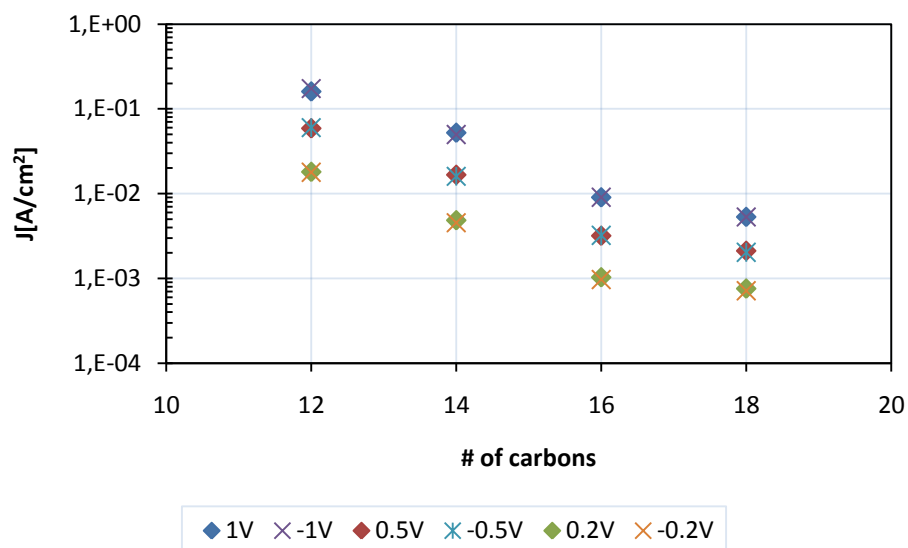


Figure 40. J values measured at 0.2V, -0.2V, 0.5V, -0.5V, 1V and -1V as a function of the chain length of the alkanethiols.

The error of the β coefficient at 1V was $0.60 n_c^{-1} \pm 0.11$. The highest possible β is $0.71 n_c^{-1}$ and the lowest β is $0.49 n_c^{-1}$.

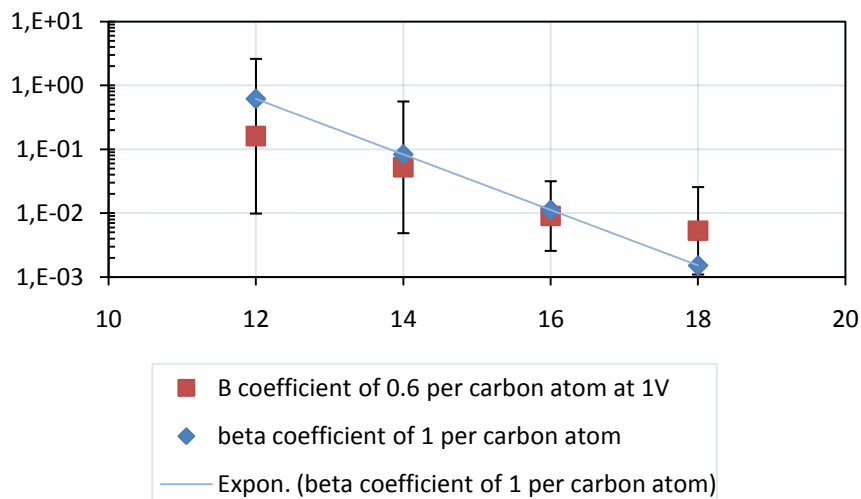


Figure 41. Plot of the current densities at 1 V +/- 1 standard deviation as a function of the chain length of alkanethiols (contact areas are between 400 and 100 μm^2) (red) and an idealized plot of data points showing a tunneling decay coefficient β [n_c^{-1}] of 1 (blue). The determination of the idealized blue data points is explained in the text below.

Figure 41 shows the J versus the SAM thickness for junction small junction areas and an idealized plot revealing a β coefficient of 1 n_c^{-1} . The idealized current densities for a β coefficient of 1 n_c^{-1} were determined by: $J = J_0 \exp(-\beta d) \Rightarrow J = 10^5 \exp(-d)$ where $d=12, 14, 16$ and 18 respectively. This plot allows of course only vague conclusions as by varying the J_0 value the position of the idealized data points also change. A trend that can be seen from the plot is that the values for C_{14} and C_{16} would lie on a trendline with a β coefficient of 1 n_c^{-1} but that the current densities for C_{12} and C_{18} are too low and too high respectively.

J - V curves of Au-Au junctions were measured to get information about the current density of Au-Au contacts without SAM fabricated with wedging transfer. A 10 μm top electrode was applied on top of bottom electrodes with widths between 200 and 10 μm . The results are shown in Figure 42.

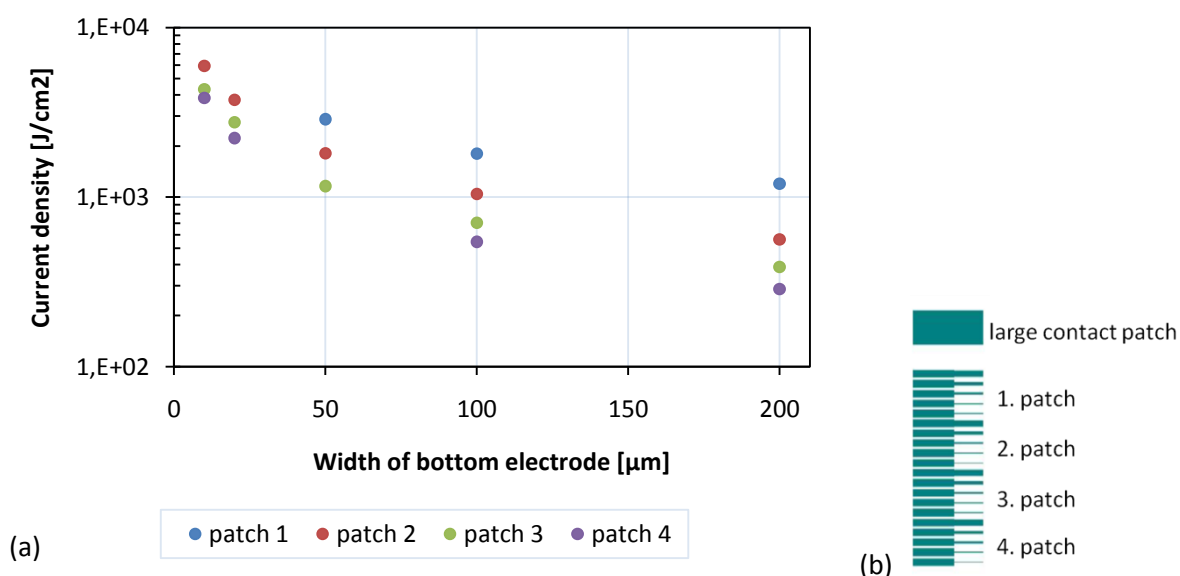


Figure 42. (a) Current density at 1V of an Au-Au junction fabricated with wedging transfer as a function of the width of the bottom contacts; the top electrode was 10 μm ; (b) Structure of the bottom contacts.

One can see that J decreases with the distance of the contact area from the large contact patch. Patch 1 is closest to the contact patch like shown in Figure 42 (b). The resistance increases with increasing length of the top electrode and decreases with increasing contact area. The resistances are in the range of $k\Omega$. The lowest resistance was measured for the for the $10 \times 200 \mu\text{m}^2$ contact on the first patch with 42Ω . The highest resistance was 260Ω for the $10 \times 10 \mu\text{m}^2$ junction on patch 4. For molecular junctions the resistances are higher (several $M\Omega$). The differences in resistance per contact patch can therefore be neglected. It has to be mentioned that some Au-Au junctions did not show a linear I - V dependence but an asymmetrical non-linear slope as well as a much higher resistance like shown in Figure 43.

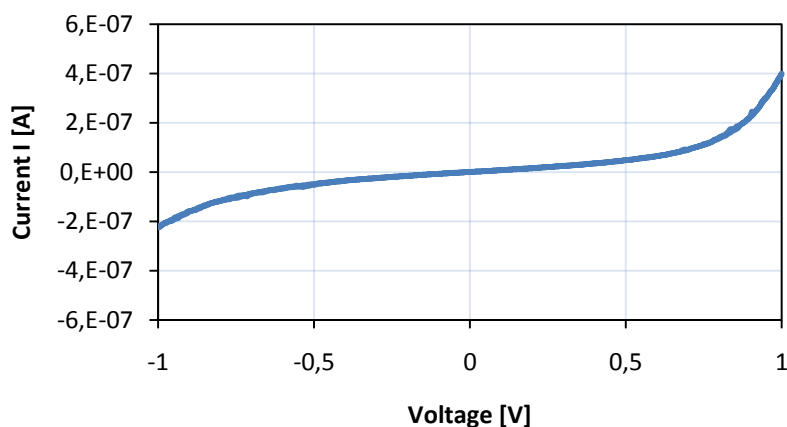


Figure 43. I - V characteristic of an Au-Au junction fabricated with wedging transfer; the contact area was $100 \mu\text{m}^2$. The asymmetrical non-linear slope and the high resistance indicate that the electrodes do not make good contact; most probably water is trapped in the junction.

These kinds of asymmetrical curves were sometimes also observed for Au-SAM-Au junctions ($\sim 2\%$). The origin of this effect is still under study. Au-SAM-Au junctions also often showed noisy I - V curves. Figure 44 shows two examples for a stable and a noisy I - V curve, respectively, of Au- C_{12} -Au junctions measured 10 times sequenced. Noisy slopes were rarely observed for molecular junctions fabricated with the original flip-chip where the top electrodes were template-stripped with a PDMS stamp as support and applied on top of the SAM¹¹. The occurrence of noisier curves for molecular junctions fabricated with wedging transfer maybe indicates the influence of water inside the junction area. If water is trapped in the junction the contact of the top electrode to the SAM is not good yielding less reliable, noisy results.

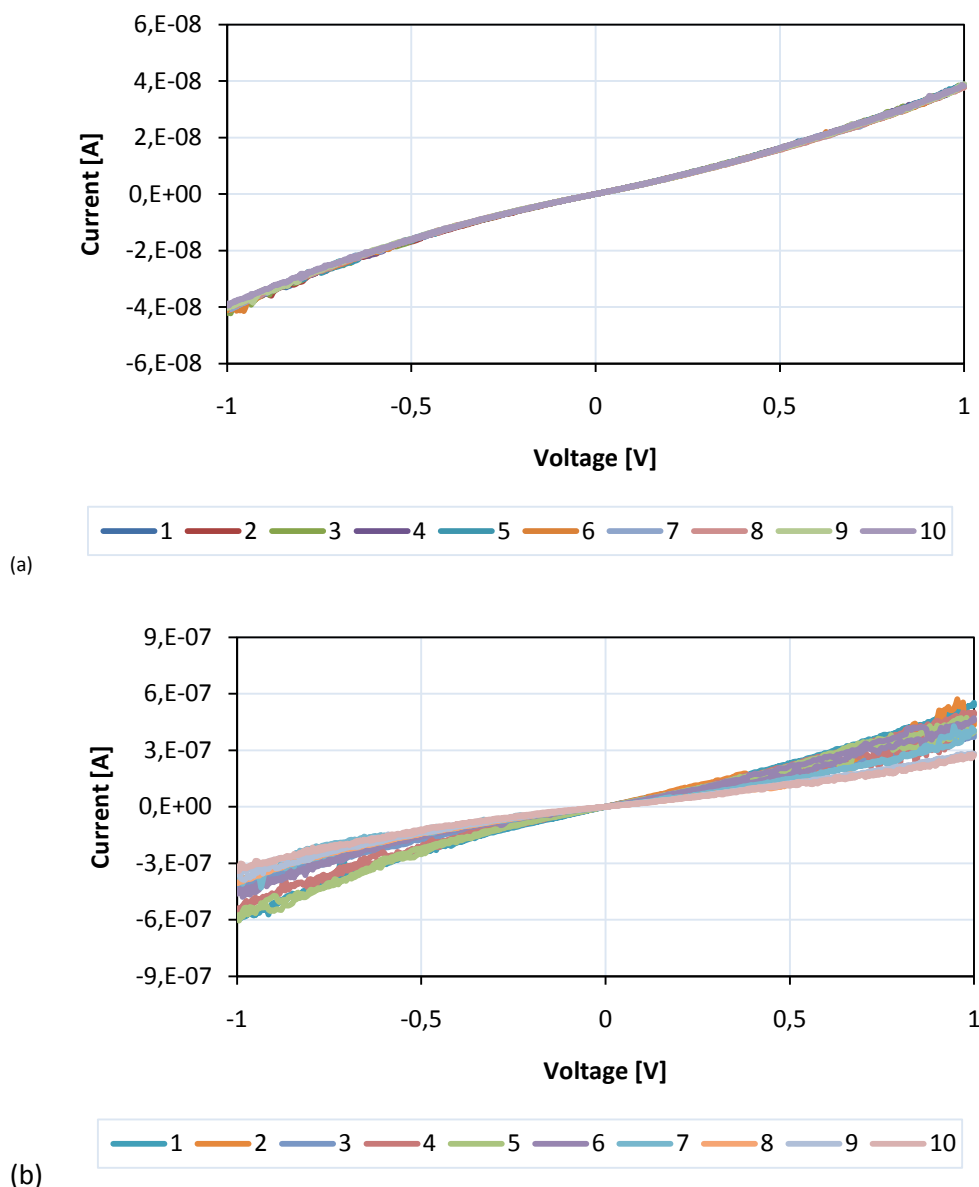


Figure 44. *I-V* characteristics of measured 10 times on the same junction. The examples illustrate a stable (a) and a noisy Au-C₁₂-Au molecular junction (b); the contact areas were 100 and 200 μm^2 respectively.

Nevertheless, despite the probability of trapped water, the working device yield was enhanced and the spread in current density was decreased with wedging transfer. The softer landing of the top electrode improved the flip-chip concept. It was possible to analyze five different lengths of SAMs and, when looking more closely into the data the exponential dependence on the number of carbon atoms in the chain of the alkanethiols was observed. Due to the huge spread in J this was not feasible before.

5. Conclusions

In this project the flip-chip concept for fabricating molecular junctions has been improved. As electrode material Au, Ag and Pt were analyzed with atomic force microscopy with regard to the rms roughness after template-stripping. It turned out that the Pt electrodes had cracks over the whole layer making it not useful for electrodes without spending time to solve this problem. Au electrodes were preferred over Ag because of their lower rms roughness and because Au is less prone to oxidation. The rms roughness was < 0.5 nm for Au and around 6 nm for Ag electrodes after template-stripping measured over an area of $2 \times 2 \mu\text{m}^2$. Probably the higher rms roughness of Ag is due to oxidation of the Ag.

The AFM images further showed that the electrodes were protruding up to 10 nm from the optical adhesive. This protrusion might be one reason for many shorts observed for flip-chip fabricated molecular junctions. Embedded electrodes are therefore favored. Au etch was tried to overcome the protrusion but the roughness of the electrodes increased and also the optical adhesive was etched. The protrusion of the electrodes thereby increased and the molecular junctions showed a low yield with a large spread in current densities. As another approach to minimize the protrusions, PMMA was spin-coated on top of the electrodes and then glued to a glass support for template-stripping. Template-stripping was also possible with PMMA. It was found that this method reduces the protrusions down to 0 - 2 nm. However, swelling of PMMA was observed when immersing it into the ethanolic thiol solution overnight for monolayer formation.

During electrode fabrication some residual photoresist was observed at the electrode edges after lift-off, this was solved by using a positive resist stripper instead of acetone. Another advantage of the resist stripper is that the Si wafer becomes more hydrophilic, which is needed for utilizing wedging transfer as a method for applying the top contact on top of the SAMs.

Wedging transfer was tried as a soft method to apply top electrodes. A soft landing of the contacts is favored in order to avoid damage to the monolayer. A special set-up was made consisting of a micromanipulator and a syringe pump. With this technique the working device yield was significantly enhanced to $\sim 40\%$ (Table 8) and also the spread in current density was decreased from 6 orders of magnitude¹¹ to about 1 - 3.5 orders of magnitude (Figure 38). The combination of the flip-chip concept with wedging transfer allows electrical characterization of SAMs in a short period of time. The yield and spread in J permit statistical electrical analysis of five alkane-monothiols differing in their molecular length. By looking at J as a function of the number of carbons in the chain, an exponential dependence was observed, as expected for tunneling conduction. This shows that the measured currents are primarily determined by the thickness of the SAMs. The tunneling decay coefficient β was measured to be $0.60 \text{ n}_c^{-1} \pm 0.11$, which is lower than the β values reported in literature (between 0.71 and 1.1 n_c^{-1})⁹. The lower value might be due to remaining water in the junction. The average current densities of alkane-monothiol junctions at 0.5 V reported in literature have a mutual spread of up to eight orders of magnitude (see Table 2). Our measured current densities are positioned approximately halfway in between the reported values.

6. Recommendations

Although the working device yield and the spread in current densities have been significantly improved by achieving a soft landing of the top contact, there are still approaches left for further advancement. First of all, it is recommended to repeat the measurements with purified thiols. The contact angles measured for the SAMs were not perfect indicating many defects in the monolayer. This could be one reason for the spread in current densities. If the spread stays the same, the monolayer quality did not cause the spread in J .

Furthermore, it can be tried to fabricate electrodes with Pt. This metal showed cracks in the 100 nm thick layer and in this project no further effort was done to solve the problem. Most probably, template-stripped Pt electrodes will have an even lower rms roughness, which is very important for high-quality SAM formation. Blackstock *et al.*³⁵ reported template-stripped Pt with sub-Ångstrom rms roughness. The p-type Si wafer with a native oxide layer is piranha (1:3) cleaned to remove all organic contaminations and to increase the oxide layer. The oxide layer is very important to allow template-stripping of Pt as it prohibits bonding between the Pt and the Si at the interface. After piranha treatment the wafer is rinsed with DI water and spin-dried. A 100 nm thick Pt layer is immediately sputtered with a rate of 5-8 nm/min. The glass slides are applied with an epoxy (EPO-TEK 377), which is cured for 2 hours at 150°C.

In the following sections, two approaches are given to further enhance the yield and to lower the spread in current density for Au-SAM-Au junctions. On the one hand the measurement conditions can be optimized and on the other hand the fabrication scheme can be further improved.

6.1. Electrical measurements under vacuum

Storing the molecular junctions after wedging transfer in a desiccator under vacuum is perhaps not enough to remove all residual water. The remaining water could also be one reason for the spread in current density and the asymmetrical I - V curves that were sometimes observed. Measuring under vacuum might remove remaining water and thereby yield more reliable measuring conditions. First tests did not show a significant difference, but the used molecular junctions were already two months old allowing no reliable conclusion.

The molecular junctions showed an exponential dependence on the SAM thickness, which is an indication for tunneling transport. To prove that the transport behavior through the alkanethiols is tunneling temperature dependent measurements have to be performed.

6.2. Embedding of the electrodes with PMMA instead of optical adhesive

Spin-coating of PMMA on top of the Au bottom electrodes and subsequently applying a glass support by means of an optical adhesive resulted in less protruding electrodes after template-stripping. A protrusion between 0 and 2 nm seems very promising improvement of the flip-chip concept. Molecular junctions with protruding electrodes have a higher probability to be shorted, because the SAM formation is not good at the edges.

Unfortunately, a swelling of PMMA was observed when immersing it into the ethanolic thiol solution overnight for monolayer formation. Like this, it is not possible to form molecular junctions with template-stripped PMMA-Au devices. A solution to this problem might be a slower cooling down (5°C/2min until RT) of the PMMA after spin-coating and baking at 120°C. Cooling down too fast makes the polymer chains become frozen in an unfavorable position. When the polymer is cooled down slower the polymer chains can arrange in their favored position. Furthermore, reducing the

UV-curing time for the OA might help to overcome the swelling as the UV light also influences the PMMA. The UV light causes polymer chain scissions due to the absorbed radiation. This de-cross-linking makes the PMMA more soluble, because the average molecular weight thereby is decreased³⁶. It is recommended to try more approaches with PMMA because of the smoother interface between PMMA-Au compared to OA-Au. A fabrication scheme is given in Appendix 2. Optical microscope images of first approaches showed no swelling although it could be that the whole layer swelled. Au electrodes embedded in PMMA therefore have to be critically analyzed.

Appendix 1

The Au electrodes are fabricated with photolithography. The negative photoresist TI 35 ES (MicroChemicals) is spin-coated on a single-side polished <100> silicon wafer with first 500 rpm (5 sec), then 4000 rpm (30 sec) and baked for 2 min at 95°C. At this state the resist would behave like an exposed positive resist where the irradiated areas are removed during the developing.

Subsequently the wafer is exposed with an inverse mask for 20 sec. An inverse mask means that the exposed areas remain after developing. Hereby a shorter exposure creates a larger undercut while a longer exposure forms steeper walls³³. In order to let the nitrogen (developed during exposure) diffuse out of the resist, the wafer is kept at room temperature for at least 30 min followed by a “reversal bake” at 120°C for 2 min. The reversal bake causes cross-linking of the irradiated area, while the unexposed area stays photo-active.

In the next step a flood full wafer exposure is performed for 60 sec. Hereby, the parts of the resist layer that were not exposed during the first exposure step, become soluble in the developer. The last lithography step is the developing in OPD4262 for 60 sec to remove the unirradiated area and subsequently quick dump rinsing with Milli-Q water. In the case of a negative resist the areas that are unirradiated will be removed during the developing step.

Before metal evaporation the wafer is cleaned for 30 min with UV-ozone. Immediately after this cleaning step 100 nm Au are evaporated (Film evaporator Balzers BAK 600) with a deposition rate of 2 to 4 Å/s.

Metal lift-off is done by placing the wafer for 60 min in a positive resist stripper (PRS 2000). Afterwards the wafer is gently washed in DI water followed by spin-drying.

The bottom electrodes are template-stripped³¹ from the wafer by using a glass slide as supporter which is glued to the wafer with an optical adhesive. Before applying the OA an anti-sticking layer (PFDTs) is deposited from gas phase for 60 min to lower the adhesion of the OA to the Si wafer. The optical adhesive is UV-cured for 2 hours. By placing a scalpel under the optical adhesive at the edge of the glass slide, the supporter including the electrodes can be gently removed from the wafer.

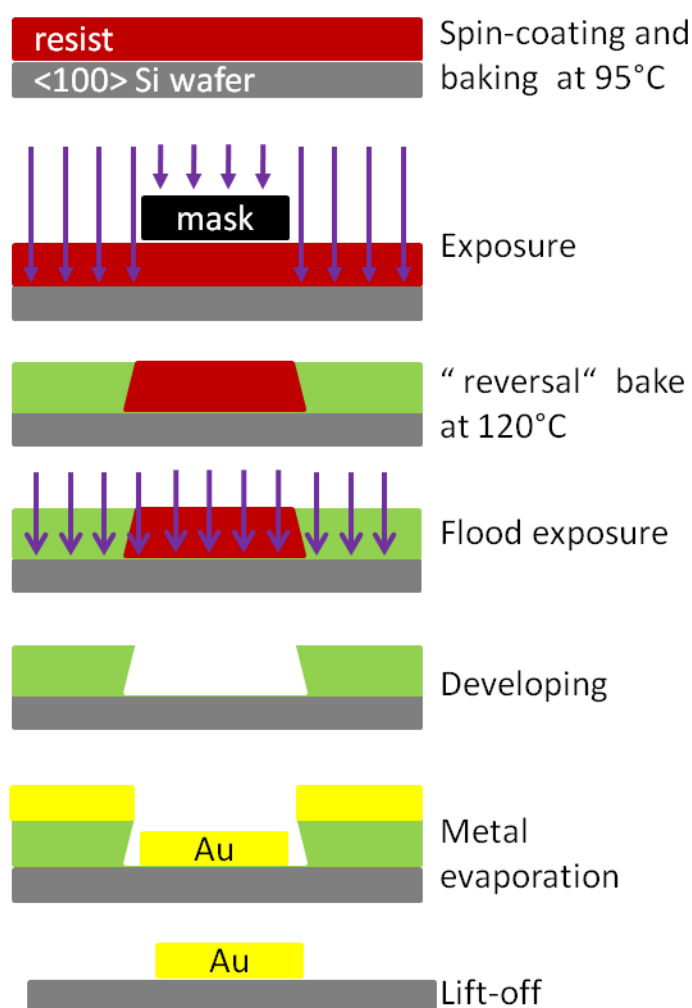


Figure 45. Schematic of the fabrication steps of metal electrodes.

For the top electrodes wedging transfer³² is utilized. Hereby, the wafer is dipped for 5 sec into cellulose acetate butyrate (30 mg/ml) in ethyl acetate including 0.1 volume % of 1-dodecanethiols. The polymer is dried under ambient conditions for 3 minutes. In order to allow a good wedging transfer the polymer is dissolved at the bottom side and at the edges of the wafer with ethyl acetate so that only the part with the electrodes is covered. The wafer is then slowly dipped into Milli-Q water under an angle of about 70°. The cellulose acetate butyrate film including the gold electrodes lifts off from the wafer and floats on the water. By lowering the water level the top electrode can be aligned on the bottom contacts covered with the SAM.

Appendix 2

The fabrication scheme for Au bottom electrodes embedded in PMMA is illustrated in Figure 46. The wafer is patterned with the negative photoresist TI 35 ES. The Ti 35 ES is spin-coated with recipe 4000 DYN (5 sec 500, then 4000 rpm). Then the wafer is baked for 2 min at 95°C followed by an exposure for 20 sec with a photomask. To let the nitrogen diffuse out of the resist, the wafer is kept untouched for >30min and then baked at 120°C for 2min. A flood exposure without mask is done, after which the wafer is developed in OPD4262 for 60 sec. In the last step the wafer is rinsed with DI water and spin-dried.

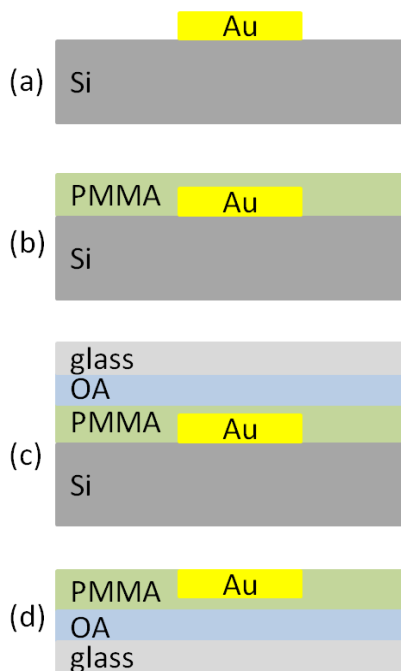


Figure 46. Fabrication steps for template-stripped bottom electrodes embedded in PMMA.

(Figure 46 c).

In the last step the Au electrodes are template-stripped from the wafer (Figure 46 d). A scalpel is placed under the PMMA and the glass slide including the electrodes embedded in PMMA is gently removed from the wafer.

A 100 nm thick Au layer is evaporated on the patterned Si wafer which was cleaned for 30 min with UV-ozone before deposition. The evaporation speed is between 2-4 Å/sec. Metal lift-off is done with the positive resist stripper PRS 2000 for 1 hour followed by gently rinsing with DI water (Figure 46 a).

An anti-sticking layer is formed to lower the adhesion between PMMA and the Si wafer. Therefore, 0.05 ml of PFDTs is placed in a desiccator together with the Au patterned wafers. The desiccator is pumped down for 10 min. The wafers are fluorinated by gas phase deposition of the PFDTs for 60 minutes.

PMMA with a molecular weight of 350 kD (6 wt% in toluene) is spin-coated with recipe 3000 DYN (5 sec 500, then 3000 rpm) (Figure 46 b). The wafer is baked at 120°C for 1 min and then cooled down to room temperature with steps of 5°C/2min. The PMMA is activated with ~20sec plasma oxidation to enhance the adhesion between the PMMA and the optical adhesive which is important to achieve reliable template-stripping. The optical adhesive is needed to glue the glass slide (cleaned with piranha) to the device. The OA is cured for 30 min

References

- 1 Aviram, A. & Ratner, M. A. Molecular rectifiers. *Chemical Physics Letters* **29**, 277-283, doi:10.1016/0009-2614(74)85031-1 (1974).
- 2 McCreery, R. L. & Bergren, A. J. Progress with Molecular Electronic Junctions: Meeting Experimental Challenges in Design and Fabrication. *Advanced Materials* **21**, 4303-4322, doi:10.1002/adma.200802850 (2009).
- 3 Moore, G. E. Cramming more components onto integrated circuits. *Electronics* **38** (1965).
- 4 Moore, G. E. in *Electron Devices Meeting, 1975 International*. 11-13.
- 5 Bruinink, C. M. *Patterning strategies in nanofabrication : from periodic patterns to functional nanostructures* Ph.D. thesis thesis, University of Twente, (2009).
- 6 Love, J. C., Estroff, L. A., Kriebel, J. K., Nuzzo, R. G. & Whitesides, G. M. Self-Assembled Monolayers of Thiolates on Metals as a Form of Nanotechnology. *Chemical Reviews* **105**, 1103-1170, doi:10.1021/cr0300789 (2005).
- 7 Li, X. *et al.* Conductance of Single Alkanedithiols: Conduction Mechanism and Effect of Molecule-Electrode Contacts. *Journal of the American Chemical Society* **128**, 2135-2141, doi:10.1021/ja057316x (2006).
- 8 Kim, T. W., Wang, G., Lee, H. & Lee, T. Statistical analysis of electronic properties of alkanethiols in metal-molecule-metal junctions. *Nanotechnology* **18** (2007).
- 9 Thuo, M. M. *et al.* Odd-even effects in charge transport across self-assembled monolayers. *Journal of the American Chemical Society* **133**, 2962-2975 (2011).
- 10 Akkerman, H. B., Blom, P. W. M., De Leeuw, D. M. & De Boer, B. Towards molecular electronics with large-area molecular junctions. *Nature* **441**, 69-72 (2006).
- 11 Krabbenborg, S. *Molecular Junctions Fabricated with the Flip-chip concept* MSc thesis, University of Twente, (2009).
- 12 Akkerman, H. B. *Large-Area Molecular Junctions*, <<http://dissertations.ub.rug.nl/faculties/science/2008/h.b.akkerman>> (2008).
- 13 Ulman, A. Formation and Structure of Self-Assembled Monolayers. *Chemical Reviews* **96**, 1533-1554, doi:10.1021/cr9502357 (1996).
- 14 Ulman, A. *An Introduction to Ultrathin Organic Films From Langmuir-Blodgett to Self-Assembly*. (American Press, INC., 1991).
- 15 Schreiber, F. Structure and growth of self-assembling monolayers. *Progress in Surface Science* **65**, 151-257, doi:Doi: 10.1016/s0079-6816(00)00024-1 (2000).
- 16 Nijhuis, C. A., Reus, W. F., Barber, J. R., Dickey, M. D. & Whitesides, G. M. Charge Transport and Rectification in Arrays of SAM-Based Tunneling Junctions. *Nano Letters* **10**, 3611-3619, doi:10.1021/nl101918m (2010).
- 17 Wang, W., Lee, T. & Reed, M. A. Electronic transport in self-assembled alkanethiol monolayers. *Physica E: Low-Dimensional Systems and Nanostructures* **19**, 117-125 (2003).
- 18 Seong, H. C., Kim, B. & Frisbie, C. D. Electrical resistance of long conjugated molecular wires. *Science* **320**, 1482-1486 (2008).
- 19 Hines, T. *et al.* Transition from tunneling to hopping in single molecular junctions by measuring length and temperature dependence. *Journal of the American Chemical Society* **132**, 11658-11664 (2010).
- 20 Karthäuser, S. Control of molecule-based transport for future molecular devices. *Journal of Physics Condensed Matter* **23** (2011).
- 21 Salomon, A. *et al.* Comparison of Electronic Transport Measurements on Organic Molecules. *Advanced Materials* **15**, 1881-1890, doi:10.1002/adma.200306091 (2003).
- 22 Bang, G. S. *et al.* High-fidelity formation of a molecular-junction device using a thickness-controlled bilayer architecture. *Small* **4**, 1399-1405 (2008).
- 23 Van Hal, P. A. *et al.* Upscaling, integration and electrical characterization of molecular junctions. *Nature Nanotechnology* **3**, 749-754 (2008).
- 24 Vilan, A. & Cahen, D. Soft contact deposition onto molecularly modified GaAs. Thin metal film flotation: Principles and electrical effects. *Advanced Functional Materials* **12**, 795-807 (2003).

- 25 Stein, N. *et al.* Nondestructive contact deposition for molecular electronics: Si-alkyl//Au junctions. *Journal of Physical Chemistry C* **114**, 12769-12776 (2010).
- 26 Bonifas, A. P. & McCreery, R. L. Soft Au, Pt and Cu contacts for molecular junctions through surface-diffusion-mediated deposition. *Nature Nanotechnology* **5**, 612-617 (2010).
- 27 Chiechi, R. C., Weiss, E. A., Dickey, M. D. & Whitesides, G. M. Eutectic gallium-indium (EGaIn): A moldable liquid metal for electrical characterization of self-assembled monolayers. *Angewandte Chemie - International Edition* **47**, 142-144 (2008).
- 28 Akkerman, H. B. *et al.* Stability of large-area molecular junctions. *Organic Electronics: physics, materials, applications* **11**, 146-149 (2010).
- 29 Van Hal, P. A. *et al.* Supplementary Information - Upscaling, integration and electrical characterization of molecular junctions. *Nature Nanotechnology* **3**, 749-754 (2008).
- 30 Wang, G., Kim, Y., Choe, M., Kim, T. W. & Lee, T. A new approach for molecular electronic junctions with a multilayer graphene electrode. *Advanced Materials* **23**, 755-760 (2011).
- 31 Weiss, E. A. *et al.* Si/SiO₂-templated formation of ultraflat metal surfaces on glass, polymer, and solder supports: Their use as substrates for self-assembled monolayers. *Langmuir* **23**, 9686-9694 (2007).
- 32 Schneider, G. F., Calado, V. E., Zandbergen, H., Vandersypen, L. M. K. & Dekker, C. Wedging transfer of nanostructures. *Nano Letters* **10**, 1912-1916 (2010).
- 33 MicroChemicals. TI 35ES technical data sheet (revised 10/2003).
- 34 Bain, C. D. *et al.* Formation of monolayer films by the spontaneous assembly of organic thiols from solution onto gold. *Journal of the American Chemical Society* **111**, 321-335, doi:10.1021/ja00183a049 (1989).
- 35 Blackstock, J. J., Li, Z., Freeman, M. R. & Stewart, D. R. Ultra-flat platinum surfaces from template-stripping of sputter deposited films. *Surface Science* **546**, 87-96, doi:10.1016/j.susc.2003.09.039 (2003).
- 36 Johnstone, R. W., Foulds, I. G. & Parameswaran, M. Deep-UV exposure of poly(methyl methacrylate) at 254 nm using low-pressure mercury vapor lamps. *Journal of Vacuum Science and Technology B: Microelectronics and Nanometer Structures* **26**, 682-685 (2008).

Acknowledgements

First of all I would like to thank my committee members for guiding me through this interesting Master Project.

Special thanks go to you, Sven, for the great supervision. After giving me a comprehensive introduction to all fabrication steps, you gave me the opportunity to work independently which I really appreciated. It was always possible to ask you any kind of question. I liked our discussions about arising fabrication difficulties and measurement results. I learned a lot from you and the project would not have been where it is now without your help and involvement.

I also want to thank you very much, Wilfred, for offering me this research project and for your guidance and the biweekly meetings. Your contributions were fundamental for this project. You were always available when challenges occurred.

Many thanks also to you, Jurriaan, for the guidance during the project and the regular meetings. I thank you for all the contributions and advices you gave me especially concerning the fabrication part of this project.

I would like to thank, Edwin, for being the external member of the committee and for the interesting discussions.

I am also thankful for Martin who gave me advice concerning the AFM analysis.

Moreover, I would like to thank all NE and MnF members for the great working atmosphere. The people I saw most in MnF were Pieter, Jordi, Erhan, Dodo, and Ina. You made the chemical lab a nice environment to work in. I thank the whole NE group for just being as they are. I enjoyed our NEvents and the bowling evening. Not to forget the fun we always had during lunch time. In particular I would like to thank my fellow students in the student room, Quyen, Maarten, Koert, Michel and Bernardus for making it a pleasure to work there.

I am very happy to see you all back in a few weeks!

Last but not least, I would like to thank my family for the interest and support. Especially, I thank my mum for her love and advice.